

SEGUE 2: THE LEAST MASSIVE GALAXY*

EVAN N. KIRBY^{1,2}, MICHAEL BOYLAN-KOLCHIN^{1,2}, JUDITH G. COHEN³, MARLA GEHA⁴, JAMES S. BULLOCK¹, AND MANOJ KAPLINGHAT¹

Accepted for publication in ApJ on April 21, 2013

ABSTRACT

Segue 2, discovered by Belokurov et al. (2009), is a galaxy with a luminosity of only 900 L_{\odot} . We present Keck/DEIMOS spectroscopy of 25 members of Segue 2—a threefold increase in spectroscopic sample size. The velocity dispersion is too small to be measured with our data. The upper limit with 90% (95%) confidence is $\sigma_v < 2.2$ (2.6) km s^{-1} , the most stringent limit for any galaxy. The corresponding limit on the mass within the 3-D half-light radius (46 pc) is $M_{1/2} < 1.5$ (2.1) $\times 10^5 M_{\odot}$. Segue 2 is the least massive galaxy known. We identify Segue 2 as a galaxy rather than a star cluster based on the wide dispersion in [Fe/H] (from -2.85 to -1.33) among the member stars. The stars' $[\alpha/\text{Fe}]$ ratios decline with increasing [Fe/H], indicating that Segue 2 retained Type Ia supernova ejecta despite its presently small mass and that star formation lasted for at least 100 Myr. The mean metallicity, $\langle [\text{Fe}/\text{H}] \rangle = -2.22 \pm 0.13$ (about the same as the Ursa Minor galaxy, 330 times more luminous than Segue 2), is higher than expected from the luminosity–metallicity relation defined by more luminous dwarf galaxy satellites of the Milky Way. Segue 2 may be the barest remnant of a tidally stripped, Ursa Minor-sized galaxy. If so, it is the best example of an ultra-faint dwarf galaxy that came to be ultra-faint through tidal stripping. Alternatively, Segue 2 could have been born in a very low-mass dark matter subhalo ($v_{\text{max}} < 10 \text{ km s}^{-1}$), below the atomic hydrogen cooling limit.

Subject headings: galaxies: individual (Segue 2) — galaxies: dwarf — Local Group — galaxies: kinematics and dynamics — galaxies: abundances

1. INTRODUCTION

The Sloan Digital Sky Survey (SDSS, Abazajian et al. 2009) has revolutionized the concept of a galaxy. The sky coverage and depth of SDSS enabled the discovery of low-luminosity, low-surface brightness galaxies. Because their low surface brightnesses limit the distance out to which SDSS can detect them, almost all of the new SDSS dwarfs are satellites of the Milky Way (MW). The most luminous of the new satellites, Canes Venatici I, has an absolute magnitude of $M_V = -8.6$ ($L = 2.3 \times 10^5 L_{\odot}$, Zucker et al. 2006; Martin et al. 2008), which overlaps the lower luminosity bound of the previously known satellites. The least luminous new satellite is Segue 1, with $M_V = -1.5$ ($L = 340 L_{\odot}$, Belokurov et al. 2007; Martin et al. 2008; Geha et al. 2009; Simon et al. 2011).

The extremely low luminosities and stellar masses of these galaxies prompted Willman & Strader (2012) to suggest a new definition of a galaxy to distinguish it from a star cluster. Resolved stellar spectroscopy of all of the ultra-faint ($L < 10^5 L_{\odot}$) satellites known in 2007 revealed stellar velocity dispersions far in excess of the level that would be anticipated from their stel-

lar masses alone (e.g., Simon & Geha 2007). Therefore, Willman & Strader defined a galaxy as “a gravitationally bound collection of stars whose properties cannot be explained by a combination of baryons and Newtons laws of gravity.” The definition is phrased to include cosmologies involving dark matter or post-Newtonian modifications to gravity. The definition also does not mandate *kinematic* confirmation of dark matter-like phenomenology in order to classify a star system as a galaxy. Evidence for the retention of supernova ejecta beyond what would be possible from the current baryonic mass alone can also suffice. A dispersion in heavy elements serves as proof of supernova self-enrichment and therefore as confirmation of a galaxy. The supernova self-enrichment test is important for the present work.

The low stellar densities of the SDSS ultra-faint dwarf galaxies make it difficult to detect them. These galaxies are near enough that their stellar populations are resolved. However, they contain so few stars that foreground stars and background unresolved galaxies outnumber the dwarf galaxy’s own stars. The galaxy’s stars are found instead by using matched filters, wherein only stars with appropriate colors and magnitudes are considered possible members (Rockosi et al. 2002; Walsh et al. 2009). As SDSS photometric catalogs became publicly available over the last decade, a flurry of new MW satellite galaxies were discovered using matched filters.

The first generation of SDSS (SDSS-I) has been exhausted as a discovery survey for new satellites. Additional satellites may be found by deeper surveys or by surveys that target parts of the 75% of the sky that SDSS-I did not observe. One such survey was the Sloan Extension for Galactic Understanding and Evolution (SEGUE, Yanny et al. 2009), which was part of

* The data presented herein were obtained at the W. M. Keck Observatory, which is operated as a scientific partnership among the California Institute of Technology, the University of California and the National Aeronautics and Space Administration. The Observatory was made possible by the generous financial support of the W. M. Keck Foundation.

¹ University of California, Department of Physics and Astronomy, 4129 Frederick Reines Hall, Irvine, CA 92697, USA

² Center for Galaxy Evolution Fellow.

³ California Institute of Technology, Department of Astronomy & Astrophysics, 1200 E. California Blvd., MC 249-17, Pasadena, CA 91125, USA

⁴ Yale University, Department of Astronomy, 260 Whitney Ave., New Haven, CT 06511, USA

SDSS-II. SEGUE discovered three additional satellites: the previously mentioned Segue 1, the ultra-faint galaxy Segue 2 (Belokurov et al. 2009, hereafter B09), and the globular cluster Segue 3. Segue 3 is known to be a globular cluster because it has neither kinematic evidence of dark matter nor a dispersion of metallicity (Fadely et al. 2011). Segue 2 is the subject of this article.

B09 discovered Segue 2 (also called the Aries ultra-faint dwarf) in SEGUE imaging. They obtained spectroscopy and deeper imaging with the Hectospec and Megacam instruments on the MMT. They found that Segue 2 has a luminosity of $M_V = -2.5$ ($900 L_\odot$). From the individual radial velocities of five red giants, they measured a velocity dispersion of $3.4_{-1.2}^{+2.5}$ km s⁻¹. The expected velocity dispersion in the absence of dark matter is 0.5 km s⁻¹. Hence, Segue 2 seemed to contain significantly more dark matter than luminous matter.

B09 also found tentative evidence for a stellar stream at the same position as Segue 2. It was detected as an over-density of stars at the same radial velocity as Segue 2, but with larger metallicities than the gravitationally bound stars. The stream occupies a larger area of sky than the galaxy. The presence of the stream is exciting because it could be that Segue 2 was deposited in the MW halo as a satellite or subcomponent of a larger galaxy that has been tidally disrupted. A similar origin has been proposed for stellar systems that may have arrived via the tidal dissolution of the Sagittarius dwarf galaxy (e.g., Law & Majewski 2010).

One of the most interesting properties of Segue 2 is its average metallicity. Dwarf spheroidal galaxies (dSphs) obey a universal relationship between average stellar metallicity and luminosity or stellar mass (Kirby et al. 2011b). The relation predicts that a galaxy of Segue 2’s luminosity should have $\langle[\text{Fe}/\text{H}]\rangle = -2.83$. From the coadded spectrum of five red clump giants, B09 determined their average metallicity to be $\langle[\text{Fe}/\text{H}]\rangle = -2.0 \pm 0.25$. Other MW satellites about as faint as Segue 2 also lie above the luminosity–metallicity relation (LZR). Segue 1 should have an average metallicity of $\langle[\text{Fe}/\text{H}]\rangle = -2.98$ based on the LZR, but Simon et al. (2011) measured $\langle[\text{Fe}/\text{H}]\rangle = -2.38 \pm 0.37$, and Vargas et al. (2013) measured $\langle[\text{Fe}/\text{H}]\rangle = -2.03 \pm 0.06$. Willman 1 should have $\langle[\text{Fe}/\text{H}]\rangle = -2.81$, but Willman et al. (2011) measured $\langle[\text{Fe}/\text{H}]\rangle = -2.19 \pm 0.46$. The deviations from the tight relationship between metallicity and luminosity might indicate that the faintest MW satellites are tidally stripped remnants of galaxies that were once hundreds of times more luminous. Or they could hint at a metallicity floor for galaxy evolution. It is important to measure metallicities for individual stars in Segue 2 to test whether the average metallicity for a larger sample remains above the LZR.

We observed stars in and around Segue 2 in order to enlarge the available spectroscopic sample, to refine the velocity dispersion and metallicities, and to measure detailed abundances. The main purpose of our study is to suggest possible formation and evolution mechanisms for Segue 2. How long did it take to form stars? Why does it have so few stars today? Was it always so faint? In Section 2, we describe our observations. In Section 3, we detail our method for measuring radial velocities, chemical abundances, and their uncertainties.

Because foreground stars outnumber Segue 2 stars by a large factor, we carefully consider membership in Section 4. From spectroscopy of the member stars, we measure the galaxy’s dynamical properties (Section 5) and chemical abundance pattern (Section 6). Section 7 discusses Segue 2’s relevance to dark matter physics. Finally, Section 8 summarizes our methodology and findings.

2. SPECTROSCOPIC OBSERVATIONS

We observed individual objects in the vicinity of Segue 2 with the DEIMOS spectrograph (Faber et al. 2003) on the Keck II telescope. The target density in this region of the sky allowed about 80 spectroscopic targets per slitmask.

2.1. Target selection

We placed ten slitmasks on and around the center of Segue 2. The slitmasks were contiguous on the sky. We selected targets from Data Release 7 of SDSS (Abazajian et al. 2009) by querying CasJobs, the online database tool for SDSS, for point sources classified as stars in the 30’ around Segue 2. In the instances when slitmask design constraints forced a choice among multiple objects, we chose the object that lay closest in $g - r$ color to a Yonsei-Yale theoretical isochrone (Demarque et al. 2004) with an age of 14 Gyr and $[\text{Fe}/\text{H}] = -1.5$. We chose $[\text{Fe}/\text{H}] = -1.5$ rather than $[\text{Fe}/\text{H}] = -2$ (B09) to be more inclusive of metal-rich stars. For example, a star at $[\text{Fe}/\text{H}] = -3$ is slightly bluer than the $[\text{Fe}/\text{H}] = -2$ isochrone, but a star at $[\text{Fe}/\text{H}] = -1$ is much redder. Therefore, we chose a central isochrone more metal-rich than the measured mean metallicity. In practice, the sample is almost entirely free of color or metallicity bias because the stellar density rarely forced a choice among multiple spectroscopic targets. In the cases when a brighter star lay about as close to the isochrone as a fainter star, we chose the brighter star.

Figure 1 shows a color-magnitude diagram for the region of the sky enclosed by the DEIMOS slitmasks. Figure 2 shows the slitmask placement on the sky. The area of sky covered is about 0.12 deg², which is about one sixth of the area covered by B09’s Hectospec survey. In both figures, all symbols other than the smallest dots indicate targets for which we obtained spectra. The scarcity of the smallest dots in these figures shows that we observed many of the possible member red giants, subgiants, and horizontal branch (HB) stars in Segue 2. There were 647 unique spectroscopic targets. Of these, 349 were stars with spectral quality sufficient to recover a radial velocity. Only 25 of these stars are likely members of Segue 2 (see Section 4).

One star (SDSS J021900.06+200635.2) on the HB turned out to be an RR Lyrae star. Boettcher et al. (2013) discovered the star’s variability with multi-epoch photometry of Segue 2. Because RR Lyrae stars vary in their observed radial velocity by 50–70 km s⁻¹ even in the weak metal lines (Preston & Paczynski 1964; Sesar 2012), we excluded SDSS J021900.06+200635.2 from the measurement of the velocity dispersion. We also excluded it from the measurement of chemical abundances because the metal lines of RR Lyrae stars are too weak

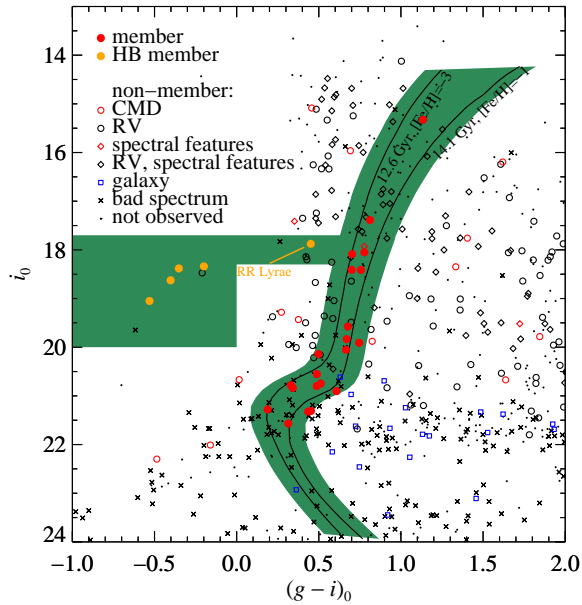


Figure 1. Color-magnitude diagram from SDSS (Abazajian et al. 2009) for the 160 arcmin² of sky centered on Segue 2 (same area shown in Figure 2). The figure legend lists reasons for which stars were excluded from consideration as members. Additionally, stars outside of the shaded region, which is based on Yonsei-Yale theoretical isochrones (Demarque et al. 2004), are ruled non-members. The black curves show isochrones of two different ages and metallicities. Filled circles are member stars. Red/orange (black) symbols identify stars that passed (failed) the radial velocity test. Diamonds indicate stars that show spectral features, such as a strong Na I 8190 doublet, indicating that they are foreground dwarfs. Blue squares indicate spectroscopically identified galaxies.

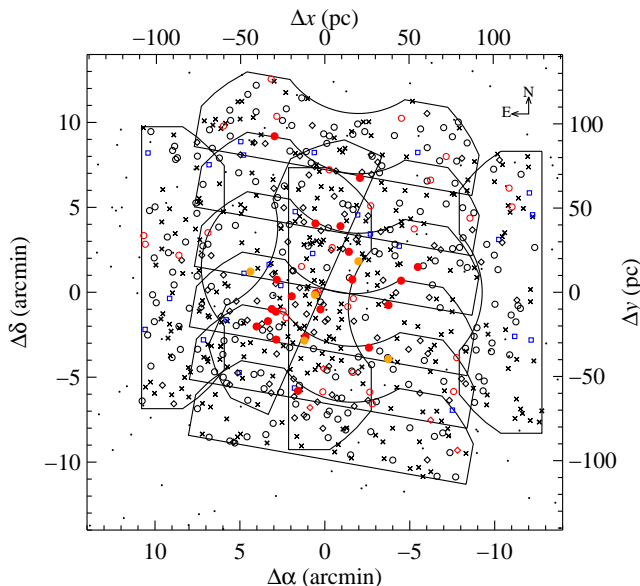


Figure 2. Sky map centered on Segue 2 ($\alpha_0 = 2^{\text{h}}19^{\text{m}}16^{\text{s}}$, $\delta_0 = +20^{\circ}10'31''$, B09). The outlines of the ten DEIMOS slitmasks enclose the objects observed. The symbols have the same meanings as in Figure 1.

for medium-resolution spectroscopy and because RR Lyrae stars are best observed at a specific phase to obtain high-resolution spectroscopic abundances (Preston

1964; For et al. 2011).

2.2. Observations

We observed the slitmasks in generally excellent weather during three nights in 2009 and one night in 2013. Table 1 details the exposure times for and conditions under which each slit each slitmask was observed.

We obtained calibration exposures in the afternoons before each observing night. These included three quartz flat lamp exposures and one arc lamp exposure per slitmask. The arc lamp exposures included simultaneous Ne, Ar, Kr, and Xe lamps.

Slitmasks were aligned with a minimum of four 4'' alignment boxes. Seeing was measured from the FWHM of the profiles of the alignment stars when the grating was angled for zeroth order (no spectral dispersion). Spectral observations were obtained with the 1200 line mm⁻¹ grating in first order. The resolution in this configuration was 1.2 Å FWHM, corresponding to a resolving power of $R = 7000$ at the Ca II infrared triplet. The grating has a blaze wavelength of 7760 Å, and we set the central wavelength to 7800 Å. Vignetting near the edges of the field of view and the locations of slits along the dispersion axis caused variation in the wavelength coverage from slit to slit by up to 300 Å. The typical wavelength range for a single object was 2700 Å. During spectral observations, DEIMOS's active flexure compensation system kept the spectra stationary on the detector within a precision of 0.07 Å in the dispersion direction and 0''.02 in the spatial direction.

2.3. Reductions

We reduced the raw images into one-dimensional spectra with the `spec2d` software (Cooper et al. 2012) developed by the Deep Extragalactic Evolutionary Probe 2 team (DEEP2, Davis et al. 2003; Newman et al. 2013). Small modifications to the pipeline allowed for better extraction of 1-D spectra by treating the stars as point sources rather than extended galaxies. For a slightly more detailed description of the data reduction procedure, see Section 2.3 of Kirby et al. (2012), who used DEIMOS in the same configuration.

Figure 3 shows three examples of reduced 1-D spectra at a variety of signal-to-noise ratios (S/Ns). All three stars were determined to be members (Section 4). The quality of the top two spectra is high enough to measure both radial velocities (Section 3.1) and chemical abundances (Section 3.3). The quality of the bottom spectrum is good enough to measure its radial velocity but not metallicity or chemical abundance ratios to the required precision.

3. SPECTROSCOPIC MEASUREMENTS

From the reduced 1-D spectra, we measured stellar radial velocities and chemical abundances. The procedures for both measurements closely mimic those described by Kirby et al. (2012). Please refer to that article for details not included here.

3.1. Radial Velocity Measurements

We cross-correlated each 1-D spectrum with template spectra obtained by Simon & Geha (2007). We adopted

Table 1
DEIMOS Observations

Slitmask	# targets	Date	Airmass	Seeing (")	Individual Exposures (s)	Total Exposure Time (s)
Ari-2	85	2009 Feb 19	1.29	0.8	1200 + 1600	2800
seg2_1	89	2009 Oct 13	1.22	0.6	3 × 1200	3600
seg2_2	91	2009 Oct 13	1.03	0.6	4 × 1200	4800
seg2_3	86	2009 Oct 13	1.22	0.6	3 × 1200	3600
seg2_4	81	2009 Oct 14	1.50	0.5	3 × 1200 + 534 + 700	4834
seg2_5	83	2009 Oct 14	1.08	0.4	4 × 1200	4800
seg2_6	84	2009 Oct 14	1.03	0.5	4 × 1200	4800
seg2_7	83	2009 Oct 13	1.20	0.5	3 × 1200	3600
seg2_8	69	2009 Oct 14	1.18	0.6	3 × 1200	3600
seg2_9	29	2013 Jan 13	1.03	1.2	6 × 1200	7200

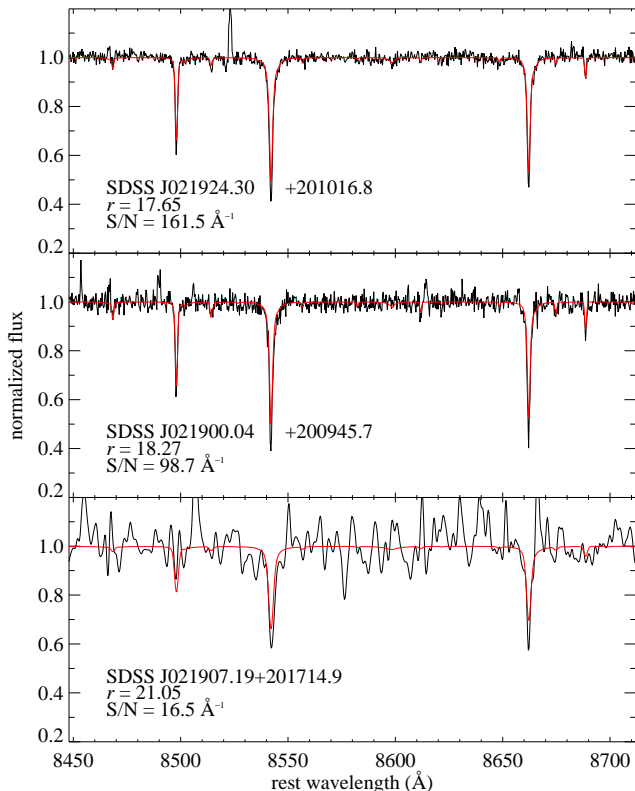


Figure 3. Examples of small regions of DEIMOS spectra of three member stars of high, medium, and low S/N. In the top two panels, the best-fitting synthetic spectra are plotted in red. The spectral fitting for chemical abundances excludes the poorly modeled Ca triplet. Because the S/N of the spectrum in the bottom panel is too low to fit a synthetic spectrum, the red line shows a synthetic spectrum with parameters representative of a subgiant in Segue 2. The spectra in the bottom panel are smoothed with a Gaussian kernel of 1.6 Å FWHM.

the radial velocity (v_r) at the cross-correlation peak of the template spectrum with the lowest χ^2 when compared to the observed spectrum. All of the radial velocities were checked by visually comparing the template spectrum to the velocity-corrected observed spectrum. Because astrometric uncertainty and imperfect slitmask alignment can cause a star to be mis-centered in its DEIMOS slitlet, we also applied a correction to v_r based on the observed wavelengths of telluric absorption bands. Sohn et al. (2007) first applied this technique

to DEIMOS spectra. For each DEIMOS spectrum, we cross-correlated the observed A and B molecular absorption bands imprinted by the Earth’s atmosphere with the template spectrum of a hot star. We then applied a correction to v_r to align the telluric bands of each observed spectrum with the template spectrum. Finally, we shifted all velocities to the heliocentric frame. All velocities quoted in this article are heliocentric velocities (v_{helio}).

We estimated uncertainties on v_r by resampling the spectrum and repeating the cross-correlation. The `spec2d` reduction software produced an estimate of the noise in each pixel. We added Gaussian random noise to each spectrum based on this array. This process degraded the S/N by $\sqrt{2}$. We measured v_r from the noise-added array. Then, we resampled the spectrum with a different Gaussian random noise array. In all, we measured v_r from 1000 realizations of the spectrum. The random radial velocity uncertainty from the Monte Carlo resampling, $\delta_{\text{MC}}v_r$, is the standard deviation of the 1000 measurements of v_r .

Simon & Geha (2007) found that $\delta_{\text{MC}}v_r$ is an incomplete description of the error on v_r . In particular, they found a systematic error floor of $\delta_{\text{sys}}v_r = 2.2 \text{ km s}^{-1}$. The systematic error is added in quadrature with the random uncertainty such that the total error on v_r is $\delta v_r = \sqrt{\delta_{\text{MC}}v_r^2 + \delta_{\text{sys}}v_r^2}$. Simon & Geha estimated this error from 49 repeat measurements of v_r for the same stars on different DEIMOS slitmasks. From a different set of 106 repeat observations in the galaxy VV124, Kirby et al. (2012) calculated $\delta_{\text{sys}}v_r = 2.21 \text{ km s}^{-1}$. Our data set for Segue 2 includes 35 measurements that satisfy all membership cuts (Section 4) except radial velocity. From these 35 stars, we calculated $\delta_{\text{sys}}v_r = 1.95 \text{ km s}^{-1}$. Because this estimate of systematic error was determined from the same data set, we used it for the remainder of our analysis. We also repeated our analysis adopting $\delta_{\text{sys}}v_r = 2.2 \text{ km s}^{-1}$. The slightly larger systematic error did not change any of our qualitative conclusions, and it changed the quantitative limits we placed on the velocity dispersion and mass by only a few percent.

Measuring v_r was not possible for many of the spectroscopic targets. The most common failure mode was low S/N, which prevented the identification of a clear cross-correlation peak. All spectra were compared to a template spectrum shifted to the radial velocity of the target star in order to verify that the cross-correlation

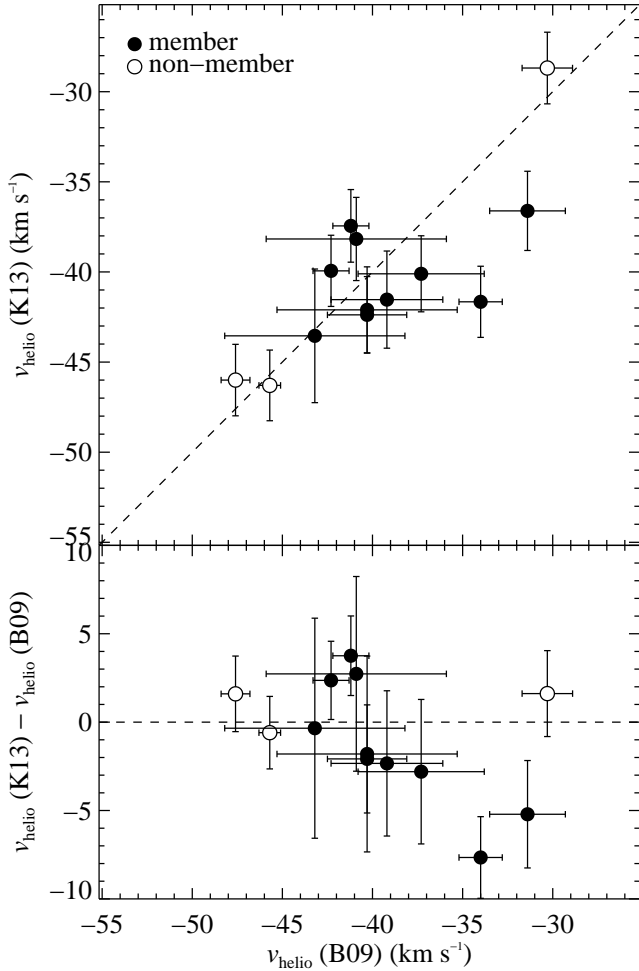


Figure 4. Comparison of radial velocities from this work to B09. The velocities of all of the stars agree to within the combined 2σ errors. Of the 13 stars, 9 agree to within the 1σ errors. B09 classified the three non-member stars as stream members.

succeeded. In the event that none of H α or the three strong Ca II triplet lines at 8498, 8542, or 8662 Å could be recognized, the spectrum was flagged as “Bad,” meaning that it was of insufficient quality to measure v_r confidently. Some spectra also suffered reduction problems, where large portions were missing. These spectra were also flagged as Bad. Some targets turned out to be galaxies (see Section 4.2), and we did not attempt to measure their redshifts.

In order to maximize the spectral S/N and minimize measurement errors for the 47 stars observed on multiple slitmasks, we coadded the individual spectra. The individual spectra were shifted into the same heliocentric frame before coaddition. The coaddition weighted each pixel by its inverse variance so that the S/N of the coadded spectrum was maximized. We measured radial velocities and chemical abundances from the coadded spectra.

Table 2 lists all of the spectroscopic targets and, where possible, the measurements of v_{helio} and their uncertainties. The table also includes SDSS identifications and photometry.

3.1.1. Comparison to B09

Our sample overlaps with 13 stars in B09’s sample. Figure 4 shows the comparison between our measurements of v_{helio} and theirs. All but four stars agree to within the combined 1σ uncertainties, and three of those four stars agree to within the 2σ uncertainties. Table 3 also shows the comparison between our work (K13) and B09.

3.2. Na I 8190 Doublet

The major contaminants in the Segue 2 spectroscopic sample are foreground MW dwarf stars. These stars have large surface gravities, which are reflected in the strength of some absorption lines. In the DEIMOS spectral range, the lines most affected by surface gravity are the Na I doublet at 8190 Å. Although the doublet is in a spectral region affected by telluric absorption, the equivalent width (EW) in a typical dwarf star is 1 Å, strong enough to be noticed easily through the telluric absorption.

Most spectroscopic targets did not have a detectable Na I doublet. For the rest, we measured the EW of each line in the doublet by fitting a Gaussian or a Lorentzian profile, depending on which profile better matched the observed line. The sum of the two EWs is EW(Na), which is given in Table 2. These measurements were used to rule some stars as non-members (Section 4.2).

3.3. Chemical Abundance Measurements

Kirby et al. (2008) showed that the resolution of DEIMOS spectra hardly limits the ability to measure iron abundances in red giants compared to high-resolution spectroscopy. Later, Kirby et al. (2010) demonstrated that [Fe/H] can be measured to a precision of 0.11 dex for DEIMOS spectra with high S/N. Furthermore, [Mg/Fe], [Si/Fe], [Ca/Fe], and [Ti/Fe] can be measured with comparable precision.

The abundances were measured by a χ^2 comparison of the observed spectrum to a grid of synthetic spectra. Only neutral atomic absorption lines were used. The Ca II triplet was specifically excluded. In the initial stages of the measurement, the effective temperature, surface gravity, and metallicity were based on photometry. In the case of Segue 2, we used 14 Gyr Padova isochrones (Girardi et al. 2002), which are available in the SDSS filters. In successive iterations, the temperature and metallicity were refined by fitting small spectral regions around Fe I lines. In the last steps, the four abundance ratios mentioned above were measured by restricting the spectral matching separately to neutral Mg, Si, Ca, and Ti lines.

We were able to measure [Fe/H] for 287 stars, assuming that they are all at the distance of Segue 2. At least one $[\alpha/\text{Fe}]$ abundance ratio was measurable for all but two of the 10 of those stars later determined to be members (Section 4). Those measurements are given in Table 4.

As a check on our [Fe/H] measurements, we also measured [Fe/H] from an empirical calibration based on the Ca II triplet (Starkenburg et al. 2010). For stars where the lines at 8542 and 8662 Å were observed, we fit separate Lorentzian profiles to each line. We added their EWs and applied Starkenburg et al.’s calibration. This calibration requires a V magnitude, which we calculated from the SDSS magnitudes using Jordi et al.’s (2006) metallicity-independent transformation equations.

Table 3
Comparison of Radial Velocities with Belokurov et al. (2009)

ID (SDSS)	ID (B09)	v_r		v_r (K13) - v_r (B09) (km s ⁻¹)	σ	Member?	
		K13 (km s ⁻¹)	B09 (km s ⁻¹)			K13 ^a	B09 ^{a,b}
SDSS J021904.93+200715.4	Seg2-023	-40.1 ± 2.1	-37.3 ± 3.5	-2.8 ± 4.1	-0.7	Y	Y
SDSS J021909.97+201254.0	Seg2-021	-42.4 ± 2.1	-40.3 ± 2.2	-2.1 ± 3.1	-0.7	Y	?
SDSS J021904.38+201837.4	Seg2-063	-46.3 ± 2.0	-45.7 ± 0.6	-0.6 ± 2.1	-0.3	N	S
SDSS J021900.04+200945.7	Seg2-024	-37.4 ± 2.0	-41.2 ± 1.0	+3.8 ± 2.2	+1.7	Y	Y
SDSS J021920.87+200754.0	Seg2-007	-36.6 ± 2.2	-31.4 ± 2.1	-5.2 ± 3.0	-1.7	Y	?
SDSS J021836.75+201217.8	Seg2-069	-46.0 ± 2.0	-47.6 ± 0.8	+1.6 ± 2.1	+0.7	N	S
SDSS J021918.49+201021.9	Seg2-003	-42.1 ± 2.4	-40.3 ± 5.0	-1.8 ± 5.5	-0.3	B	B
SDSS J021904.48+200218.4	Seg2-056	-28.7 ± 2.0	-30.3 ± 1.4	+1.6 ± 2.4	+0.7	N	S
SDSS J021922.71+200443.3	Seg2-033	-41.7 ± 2.0	-34.0 ± 1.2	-7.7 ± 2.3	-3.3	Y	Y
SDSS J021934.68+201144.3	Seg2-029	-43.5 ± 3.7	-43.2 ± 5.0	-0.3 ± 6.2	-0.1	B	B
SDSS J021929.33+200931.9	Seg2-016	-41.5 ± 2.7	-39.2 ± 3.1	-2.3 ± 4.1	-0.6	Y	?
SDSS J021907.59+201220.8	Seg2-011	-38.2 ± 2.3	-40.9 ± 5.0	+2.7 ± 5.5	+0.5	B	B
SDSS J021924.30+201016.8	Seg2-006	-39.9 ± 2.0	-42.3 ± 1.0	+2.4 ± 2.2	+1.1	Y	Y

^a B denotes horizontal branch stars.

^b S denotes stars that B09 classified as members of a stellar stream coincident with Segue 2. B09 considered some red giants just above the subgiant branch to be possible members, and they are denoted by a question mark (?).

Table 4
Abundances of Member Stars

ID	[Fe/H]	[Mg/Fe]	[Si/Fe]	[Ca/Fe]	[Ti/Fe]
SDSS J021904.93+200715.4	-2.29 ± 0.12	+0.71 ± 0.34	+0.09 ± 0.37
SDSS J021920.87+200754.0	-2.30 ± 0.18	...	+0.52 ± 0.40	+0.45 ± 0.38	...
SDSS J021922.71+200443.3	-2.25 ± 0.11	...	+0.46 ± 0.20	+0.30 ± 0.17	+0.40 ± 0.22
SDSS J021909.97+201254.0	-1.33 ± 0.12	+0.10 ± 0.46	-0.25 ± 0.33	...	-0.26 ± 0.43
SDSS J021917.10+200930.6	-2.20 ± 0.13	...	+0.62 ± 0.17	+0.34 ± 0.21	+0.70 ± 0.18
SDSS J021924.30+201016.8	-2.53 ± 0.12	...	+0.80 ± 0.14	+0.78 ± 0.14	+0.67 ± 0.15
SDSS J021900.04+200945.7	-1.91 ± 0.11	...	-0.05 ± 0.23	+0.27 ± 0.19	-0.10 ± 0.27
SDSS J021929.33+200931.9	-2.68 ± 0.31
SDSS J021928.04+201115.2	-2.03 ± 0.32
SDSS J021933.13+200830.2	-2.85 ± 0.11	+0.76 ± 0.25	+0.17 ± 0.25	+0.30 ± 0.13	-0.18 ± 0.31

Figure 5 shows the comparison between the Ca triplet metallicity and those from spectral synthesis of Fe I lines for those stars determined to be members by the criteria laid out in the next section. Six (60%) of the measurements agree to within the 1σ error bars. Three more (30%) agree to within 2σ . However, one star (SDSS J021904.93+200715.4) has $[\text{Fe}/\text{H}]_{\text{syn}} = -2.29 \pm 0.12$ and $[\text{Fe}/\text{H}]_{\text{CaT}} = -3.23 \pm 0.05$. Visual inspection of strong iron lines, such as Fe I 8689, showed that the synthetic fit accurately represents the Fe lines in the spectrum. Furthermore, the $[\alpha/\text{Fe}]$ ratios measured for this star fall in line with Segue 2 stars adjacent in metallicity. The $[\alpha/\text{Fe}]$ ratio would have been ~ 1 dex higher if the star truly had $[\text{Fe}/\text{H}] = -3.23$. We chose to rely on the spectral synthesis measurements rather than the Ca triplet because spectral synthesis provides independent estimates of both $[\text{Fe}/\text{H}]$ and $[\alpha/\text{Fe}]$ ratios. It also measures $[\text{Fe}/\text{H}]$ from Fe lines instead of Ca lines.

4. MEMBERSHIP

Because Segue 2 is such a sparse galaxy, it was necessary to remove contaminants from the spectroscopic sample. The primary contaminants were foreground dwarf stars. Evolved stars and galaxies also contaminated the sample. This section describes the criteria for a star to be considered a member of Segue 2.

4.1. Photometric Criteria

In the absence of better candidates for membership, many objects were placed on the DEIMOS slitmasks with the knowledge that they could not be members of Segue 2. These objects were spectroscopically targeted merely to fill the slitmasks. We ruled stars as non-members if they lay outside of a selection area in the i_0 vs. $(g-i)_0$ CMD, shown in Figure 1. The selection area was bounded on the red side of the red giant branch by a Yonsei-Yale isochrone with an age of 14.1 Gyr and $[\text{Fe}/\text{H}] = -1$. The blue bound was a Yonsei-Yale isochrone with an age of 12.6 Gyr and $[\text{Fe}/\text{H}] = -3$. In order to be more inclusive of a range of metallicities and ages and to account for modeling errors in the isochrones, an additional buffer of 0.1 mag in color was allowed beyond the blue and red isochrones. Finally, we also allowed stars on the HB in two selection boxes defined by $-1.0 < (g-i)_0 < 0.0$ and $17.7 < i_0 < 20.0$ and $0.0 \leq (g-i)_0 < 0.6$ and $17.3 < i_0 < 18.3$.

4.2. Spectroscopic Criteria

The first membership cut based on spectroscopy excluded background galaxies. If a target showed redshifted emission lines or Ca H and K absorption, we ruled it as a galaxy. This criterion eliminated many objects with $i_0 > 20$.

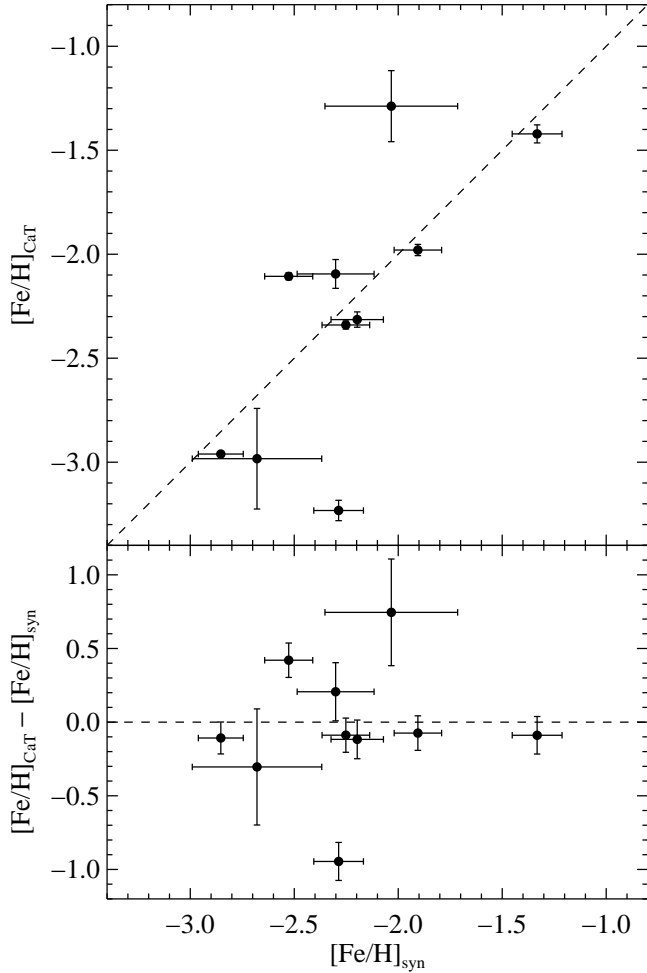


Figure 5. Comparison of iron abundances based on the Ca II triplet to iron abundances based on spectral synthesis of Fe I lines. All of the stars shown here are members of Segue 2.

Second, we identified some foreground dwarfs from EW(Na). Kirby et al. (2012) computed synthetic EWs for the Na I 8190 doublet, and they found that any star with $\text{EW}(\text{Na}) > 1 \text{ \AA}$ must be a dwarf with $\log g > 4.5$. Any stars with such high surface gravities at the distance of Segue 2 would be far too faint to be included in our spectroscopic sample. They would be foreground contaminants. We adopted the same criterion, but we also added more restrictive criteria for stars for which we measured $[\text{Fe}/\text{H}]$. Based on Kirby et al.’s (2012) Figure 6, we ruled out stars with $\text{EW}(\text{Na}) > 0.7 \text{ \AA}$ and $-2 \leq [\text{Fe}/\text{H}] < -1$. We also ruled out stars with $\text{EW}(\text{Na}) > 0.4 \text{ \AA}$ and $[\text{Fe}/\text{H}] < -2$.

Next, we imposed a metallicity cut. B09 found tentative evidence for a stellar stream coincident both in position and v_r with Segue 2. From the EW of the Mg b triplet, they found the stream to be more metal-rich than Segue 2. We recovered a metallicity of $[\text{Fe}/\text{H}] > -1$ for one star that passed all membership cuts other than metallicity. Because this star may belong to the stream, we excluded it from membership consideration.

Finally, we excluded stars based on v_{helio} . It turned out that our data cannot resolve the velocity dispersion of Segue 2. In other words, the velocity dispersion, σ_v ,

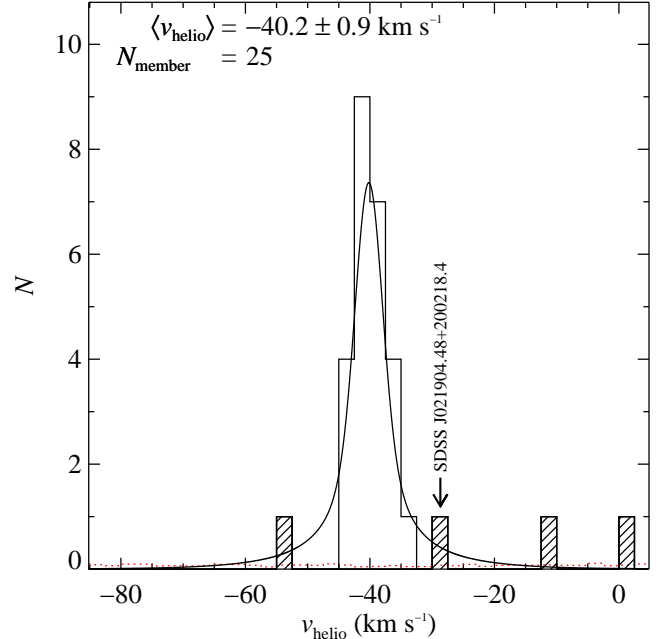


Figure 6. Radial velocity distribution of stars that pass all membership cuts except v_r . The hatched regions of the histogram show stars excluded from membership on the basis of v_r . The red, dotted histogram shows the expected level of contamination of non-members from the Besançon model. The black, solid curve shows the expected error distribution, assuming that all stars have the same intrinsic radial velocity.

is consistent with zero, such that all stars have the same intrinsic radial velocity within the measurement uncertainties. Therefore, our membership criterion based on velocity did not depend on σ_v . Instead, we accepted all stars with $|v_{\text{helio}} - \langle v_{\text{helio}} \rangle| < 2.58\delta v_r$, where $\langle v_{\text{helio}} \rangle$ is the average radial velocity, determined in Section 5. For Gaussian distributed errors, a membership cut of $2.58\delta v_r$ rejects non-members in addition to 1% of members. It is unlikely that we rejected any members with the radial velocity cut because our sample has only 25 members. Figure 6 shows the velocity distribution for stars that passed all membership cuts except radial velocity. Those stars that failed the radial velocity cut are shaded.

One star (SDSS J021904.48+200218.4) excluded on the basis of radial velocity alone had a velocity close to a member star. It is identified in Figure 6. It was excluded because the measurement uncertainty on v_{helio} was small, whereas the member star with similar velocity had a larger measurement uncertainty. The radial velocity of the non-member is 5.8σ discrepant from $\langle v_{\text{helio}} \rangle$, but the membership cut was 2.58σ . If SDSS J021904.48+200218.4 were counted as a member, Segue 2’s velocity dispersion would be $\sigma_v = 4.3 \text{ km s}^{-1}$. We are confident that it is a non-member because its velocity is highly discrepant from $\langle v_{\text{helio}} \rangle$ and because it is farther from the center of Segue 2 (8.6’ or 2.5 half-light radii) than all but one member star.

4.3. Estimate of Residual Contamination

Despite our fairly stringent membership criteria, some unidentified contaminants might have remained in our sample. The available information did not allow us to further cull the sample. Therefore, we attempted to quantify the expected level of residual contamination. In

other words, how many stars in our “member” sample are likely to be non-members?

We consulted the Besançon model of Galactic structure (Robin et al. 2003). We used their online web form⁶ to generate a catalog simulation. The simulation was limited to the galactic coordinates of the center of Segue 2. The solid angle was 10 deg², but the model parameters were based only on the coordinates of Segue 2. We chose such a large area so that the sample size was large. The model returned CFHT magnitudes, heliocentric radial velocities, and metallicities for stars in the Galactic model. The model also added mock observational uncertainties to these quantities according to a law that we determined empirically from our data set. Both photometric and kinematic errors obeyed exponential forms as a function of i_0 magnitude.

$$\delta g = -0.010 + \exp(-18.665 + 0.765i_0) \quad (1)$$

$$\delta i = -0.031 + \exp(-12.798 + 0.531i_0) \quad (2)$$

$$\delta_{\text{MC}}v_r = -0.565 + \exp(-14.730 + 0.831i_0) \quad (3)$$

We added $\delta_{\text{sys}}v_r$ in quadrature to $\delta_{\text{MC}}v_r$ to obtain δv_r , just as we did for the observed velocities. Finally, we converted CFHT to SDSS magnitudes following Regnault et al. (2009).

We applied all of the membership cuts described above to the Besançon model simulation. Just as for the observational data, we allowed model stars to pass membership cuts if colors, magnitudes, and velocities were consistent with membership. The metallicity cut needed to be modified to account for the fact that we could not recover metallicities for most faint subgiants. Therefore, a model star was eliminated based on metallicity only if it had $[\text{Fe}/\text{H}] > -1$ and $i_0 < 20.5$. That is about the magnitude where our estimated uncertainty on $[\text{Fe}/\text{H}]$ exceeded 0.4 dex. We also excluded stars with $\log g \geq 4.8$, which would have been ruled as non-members based on the Na I 8190 EW membership cut.

The model does not include Segue 2. Therefore, model stars that passed the membership cuts are called contaminants. We found 276 contaminants in the 10 deg² that we sampled from the Besançon model. This number needed to be scaled down by the actual area observed. To calculate the effective area observed, we counted the number (N_{catalog}) of objects in 0.22 deg² of the photometric catalog with $14.0 < i_0 < 20.5$ and $-1.0 < (g - i)_0 < 2.0$. We also counted the number (N_{obs}) of stars actually observed in the same magnitude and color range, reduced by the number of spectroscopically confirmed galaxies and members of Segue 2. We scaled the number of Besançon contaminants by the ratios $(0.22 \text{ deg}^2 / 10 \text{ deg}^2) \times (N_{\text{obs}} / N_{\text{catalog}})$. The result was 0.9 contaminants. The red dotted histogram in Figure 6 also shows the velocity distribution of model stars that passed all membership cuts except radial velocity. The histogram has also been scaled to reflect the expected level of contamination for the effective area of sky observed.

Contaminants could affect the measured velocity dispersion. Specifically, contaminants would cause an erroneous measurement of a resolved velocity dispersion or

cause the upper limit on the velocity dispersion to be higher. Therefore, contaminants do not affect our conclusion that we cannot resolve the velocity dispersion of Segue 2. Contaminants could also affect the chemical abundances because those measurements assumed that all stars were at the distance of Segue 2. Applied to other stars, the measurements would be meaningless. Of the member stars for which we recovered chemical abundances, none of them are nonsensical, which may indicate that these 10 stars are all true members.

4.3.1. Comparison to B09

Our spectroscopic member sample includes 21 red giants and subgiants, 4 horizontal branch stars, and 1 RR Lyrae star. The radial velocity measurements of all of the stars except the RR Lyrae star contributed to the measurement of the velocity dispersion of Segue 2. This sample size is an improvement over B09’s spectroscopic sample, which included 5 red giants, 3 subgiants, and 3 horizontal branch stars. Only the red giants contributed to their determination of the velocity dispersion. Table 3 shows the membership classification for the 13 stars in common between our two samples. Of these stars, both we and B09 classified 10 as members. We classified the remaining three stars as non-members, whereas B09 identified them as part of the putative stellar stream. B09 observed one red giant member that we did not observe. We do not disagree on the membership of any Segue 2 star.

5. DYNAMICAL PROPERTIES

We estimated $\langle v_{\text{helio}} \rangle$ and σ_v for Segue 2 using maximum likelihood statistics and a Monte Carlo Markov chain (MCMC). We maximized the logarithm of the likelihood (L) that the given values of $\langle v_{\text{helio}} \rangle$ and σ_v described the observed velocity distribution, including the uncertainty estimates for individual stars.

$$\log L = \frac{N \log(2\pi)}{2} + \frac{1}{2} \sum_i^N (\log((\delta v_r)_i^2 + \sigma_v^2)) + \frac{1}{2} \sum_i^N \left(\frac{((v_{\text{helio}})_i - \langle v_{\text{helio}} \rangle)^2}{(\delta v_r)_i^2 + \sigma_v^2} \right) \quad (4)$$

See Walker et al. (2006) for details regarding this method of measuring velocity dispersions. For initial guesses, we started with B09’s measurements: $\langle v_{\text{helio}} \rangle = -39.2 \text{ km s}^{-1}$ and $\sigma_v = 3.4 \text{ km s}^{-1}$. Then, we explored the parameter space with a Metropolis-Hastings implementation of an MCMC. The length of the chain was 10^8 trials.

The probability distribution from the MCMC is shown in Figure 7. Although $\langle v_{\text{helio}} \rangle$ is well constrained ($-40.2 \pm 0.9 \text{ km s}^{-1}$), σ_v could not be resolved. The probability increases toward zero. Therefore, we could measure only an upper limit for σ_v . Figure 8 shows the constraint on σ_v , marginalized over $\langle v_{\text{helio}} \rangle$. The upper limit on σ_v at the 90% (95%) confidence level is $\sigma_v < 2.2$ (2.6) km s^{-1} .

Our measurement of $\langle v_{\text{helio}} \rangle$ agrees with B09 to well within the measurement uncertainty. However, our measurement of σ_v is discrepant with 3.4 km s^{-1} measure-

⁶ <http://model.obs-besancon.fr>

Table 5
Properties of Segue 2

Property	Symbol	Value
Photometry		
Heliocentric distance ^a	D	35 ± 2 kpc
Galactocentric distance	D_{GC}	41 kpc
Luminosity ^a	L_V	$900 \pm 200 L_{\odot}$
Stellar mass ^b	M_*	$1000 \pm 300 M_{\odot}$
Effective (projected half-light) radius ^a	R_e	$3.4' \pm 0.2' = 34 \pm 3$ pc
3-D (deprojected) half-light radius	$R_{1/2}$	46 ± 3 pc
Dynamics		
Heliocentric mean radial velocity	$\langle v_{\text{helio}} \rangle$	-40.2 ± 0.9 km s ⁻¹
Galactocentric mean radial velocity	$\langle v_{\text{GC}} \rangle$	$+40.2$ km s ⁻¹
Line-of-sight velocity dispersion ^c	σ_v	< 2.2 (2.6) km s ⁻¹
Mass within half-light radius ^{c,d}	$M_{1/2}$	< 1.5 (2.1) $\times 10^5 M_{\odot}$
Mass-to-light ratio within half-light radius ^{c,d}	$(M/L_V)_{1/2}$	< 360 (500) M_{\odot}/L_{\odot}
Dynamical-to-stellar mass ratio within half-light radius ^{b,c,d}	$(M_{\text{dyn}}/M_*)_{1/2}$	< 300 (410)
Average density within the half-light radius ^{c,d}	$\langle \rho_{1/2} \rangle$	< 0.4 (0.5) $M_{\odot} \text{ pc}^{-3}$
Metallicity		
Mean metallicity ^e	$\langle [\text{Fe}/\text{H}] \rangle$	-2.22 ± 0.13
Standard deviation	$\sigma([\text{Fe}/\text{H}])$	0.43
Median metallicity	$\text{med}([\text{Fe}/\text{H}])$	-2.25
Median absolute deviation	$\text{mad}([\text{Fe}/\text{H}])$	0.27
Interquartile range	$\text{IQR}([\text{Fe}/\text{H}])$	0.49

References. — a: B09.

^b Assuming that $M_*/L_V = 1.2$.

^c Upper limits given as 90% (95%) C.L.

^d Using the formula $M_{1/2} = 4G^{-1}R_e\sigma_v^2$ (Wolf et al. 2010).

^e Weighted by inverse variance, following Kirby et al. (2011b).

ment at 99% confidence. We have already shown our individual radial velocity measurements to be consistent. Furthermore, we counted as members all but one of the stars that B09 counted as members. (We did not observe the other star.) The origins of the discrepancy in σ_v are the differences in sample sizes and the estimates of uncertainties on radial velocity. We used a method to determine δv_r nearly identical to B09. However, their estimate of $\delta_{\text{sys}}v_r = 0.35$ km s⁻¹ was based on low-S/N spectra in the distant Leo V ultra-faint dwarf galaxy (Walker et al. 2009). On average, B09’s velocity errors were twice as precise as those of Walker et al. (2009). Therefore, it may be that their estimate of $\delta_{\text{sys}}v_r$ was inappropriate for spectra with higher S/N. Regardless, errors in velocity measurements or underestimates of uncertainty would serve only to decrease the significance of our upper limit on σ_v . The fact that our upper limit—based on a larger sample—is lower than B09’s measurement indicates that our velocity uncertainties are not underestimated.

The measurement of σ_v can be affected by unresolved binary stars, which would artificially inflate the observed velocity dispersion. The problem is especially important for ultra-faint dwarf galaxies, where binary stars could possibly make a stellar system free of dark matter appear dark matter-dominated (McConnachie & Côté 2010). In the case of Segue 1, binaries inflate the observed velocity dispersion by 10% (Martinez et al. 2011). We compared our radial velocity measurements to those of B09. All of the radial velocities for the 10 member stars in common agree within the uncertainties. Therefore, there is no ev-

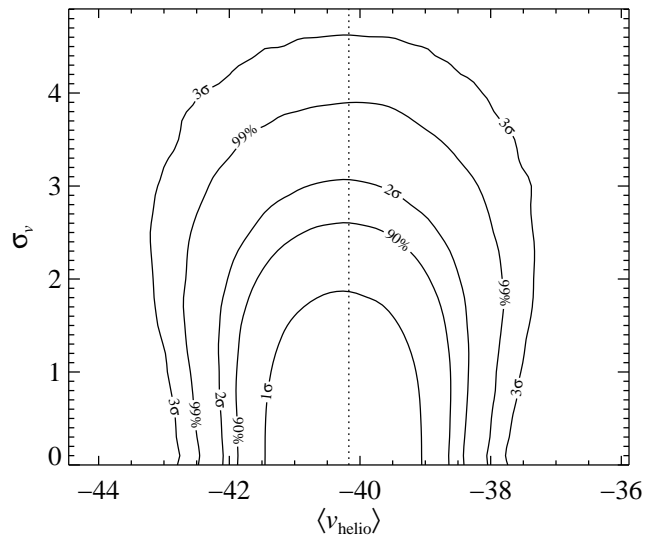


Figure 7. Probability contours for the mean velocity and velocity dispersion of Segue 2. The contours show the 1σ (68.3%), 90%, 2σ (95.4%), 99%, and 3σ (99.7%) confidence levels. The dotted line shows the maximum likelihood value of $\langle v_{\text{helio}} \rangle$.

idence for a significant inflation of the velocity dispersion by binaries. Regardless, our upper limit on the velocity dispersion is already at the limits of the precision of the radial velocities. It would be unlikely for binaries to make the velocity dispersion appear erroneously unresolved.

If Segue 2 is in equilibrium, then its total mass is re-

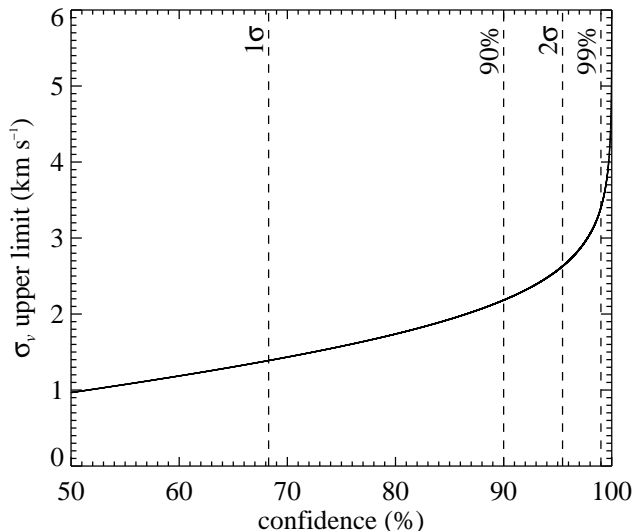


Figure 8. Upper limit on the velocity dispersion as a function of confidence level.

lated to the square of the velocity dispersion. Illingworth (1976) devised a formula appropriate for globular clusters, where the mass distribution follows the light distribution. Although this formula has been used for dwarf galaxies (e.g., Simon & Geha 2007), it typically underestimates the mass of galaxies heavily dominated by dark matter. Wolf et al. (2010) developed a similar formula appropriate for such systems. It relates the mass within the half-light radius to the velocity dispersion and the deprojected half-light radius. Because the dark matter profile is unknown, it is not possible to estimate the total mass with any accuracy, but the mass within the 3-D half-light radius (46 pc) is well constrained.

Because we could not resolve the velocity dispersion, our estimate of the mass within the half-light radius is an upper limit. At 90% (95%) confidence, that limit is $M_{1/2} < 1.5$ (2.1) $\times 10^5 M_{\odot}$. The limit on the mass-to-light ratio within the half-light radius is $(M/L_V)_{1/2} < 360$ (500) M_{\odot}/L_{\odot} .

Our upper limit on the mass of Segue 2 makes it the least massive galaxy known. Segue 2’s small mass raises the possibility that it was not always so small and that it has instead been tidally stripped by interaction with the MW. The chemical evidence also supports this scenario (Section 6.1).

The mass estimate depends on the dynamical equilibrium of Segue 2. The intrinsic line-of-sight velocity distribution for a galaxy in equilibrium should appear symmetric and roughly Gaussian. Because the velocities of all of the stars are consistent with $\langle v_{\text{helio}} \rangle$, we do not know the intrinsic shape of the velocity distribution. In the absence of a better sampled velocity distribution with smaller uncertainties, we can neither identify evidence for non-equilibrium dynamics nor conclude that the galaxy is in equilibrium and supported by dispersion. However, tidal distortion of the galaxy would tend to inflate the velocity dispersion, not depress it. It is also worth mentioning that the ellipticity of Segue 2 is small (0.15 ± 0.1 , B09), unlike other galaxies for which large ellipticities probably indicate tidal stretching and imminent destruction (e.g., Hercules, Deason et al. 2012).

The MW cannot be presently disrupting Segue 2 at its current location. Assuming a MW mass interior to Segue 2’s Galactocentric distance (41 kpc) of $10^{11} M_{\odot}$, the upper limit on the Roche radius is 1.1 kpc, which is well beyond the extent of the stars. On the other hand, if we require that the present tidal radius be twice the 3-D half-light radius, then the mass of Segue 2 would be only $80 M_{\odot}$, which is a tiny fraction of the known stellar mass. Regardless of whether tides affected Segue 2 in the past, they are not affecting it now.

Figure 9 shows various dynamical quantities for MW satellite galaxies. They are plotted versus stellar mass, which may be more relevant to these quantities, and luminosity, which is directly observable. Segue 2 is represented as the red, downward-pointing arrow in the top four panels. Despite Segue 2’s low mass, the upper limits on its dynamical quantities fall in line with the envelope defined by other dwarf galaxies. It seems to be consistent with a universal relationship between its dynamical mass and stellar mass.

Figure 9 also shows that Segue 2 has the lowest *total* mass of all of the dwarf galaxies for which the mass has been estimated. It is not the galaxy with the lowest luminosity or stellar mass. Segue 1 has a lower luminosity and a lower stellar mass than Segue 2.

5.1. Possible Stellar Stream

B09 identified a possible stellar stream at the same coordinates and radial velocity as Segue 2. The criterion for deciding stream membership rather than galaxy membership was the EW of the Mg b triplet, which is an indicator of metallicity. One of our membership cuts was that the metallicity of each star, where measurable, needed to be $[\text{Fe}/\text{H}] < -1$. The intent of this cut was to eliminate strong-lined, metal-rich foreground dwarfs as well as stream members.

Even so, we found no evidence for a tidal stream at the same position and radial velocity as Segue 2. Figure 10 shows the Ca triplet metallicity as a function of v_r . This metallicity is directly related to the EWs of the Ca II 8542 and 8662 absorption lines. Therefore, the Ca triplet metallicity is a diagnostic of stream versus galaxy membership analogous to B09’s use of the EW of the Mg b triplet. Unlike B09, we found no concentration of relatively strong-lined stars at the same velocity as Segue 2. Thus, we found no evidence for a tidal stream.

We observed three of the stars that B09 classified as stream members. We ruled all three as non-members on the basis of radial velocity. Our radial velocity cut was more restrictive than that of B09 because they included members based on a velocity dispersion of $\sigma_v = 3.4 \text{ km s}^{-1}$.

B09 found evidence for the stream with a spectroscopic sample covering an area of sky six times larger than our DEIMOS survey. The stream is less spatially concentrated than the galaxy. It is possible that our survey merely missed the stream stars.

6. CHEMICAL COMPOSITION

We measured metallicities for 10 of the 25 member stars in Segue 2. We additionally measured at least one of $[\text{Mg}/\text{Fe}]$, $[\text{Si}/\text{Fe}]$, $[\text{Ca}/\text{Fe}]$, or $[\text{Ti}/\text{Fe}]$ for 8 of those stars. Table 5 gives some of the metallicity properties of Segue 2.

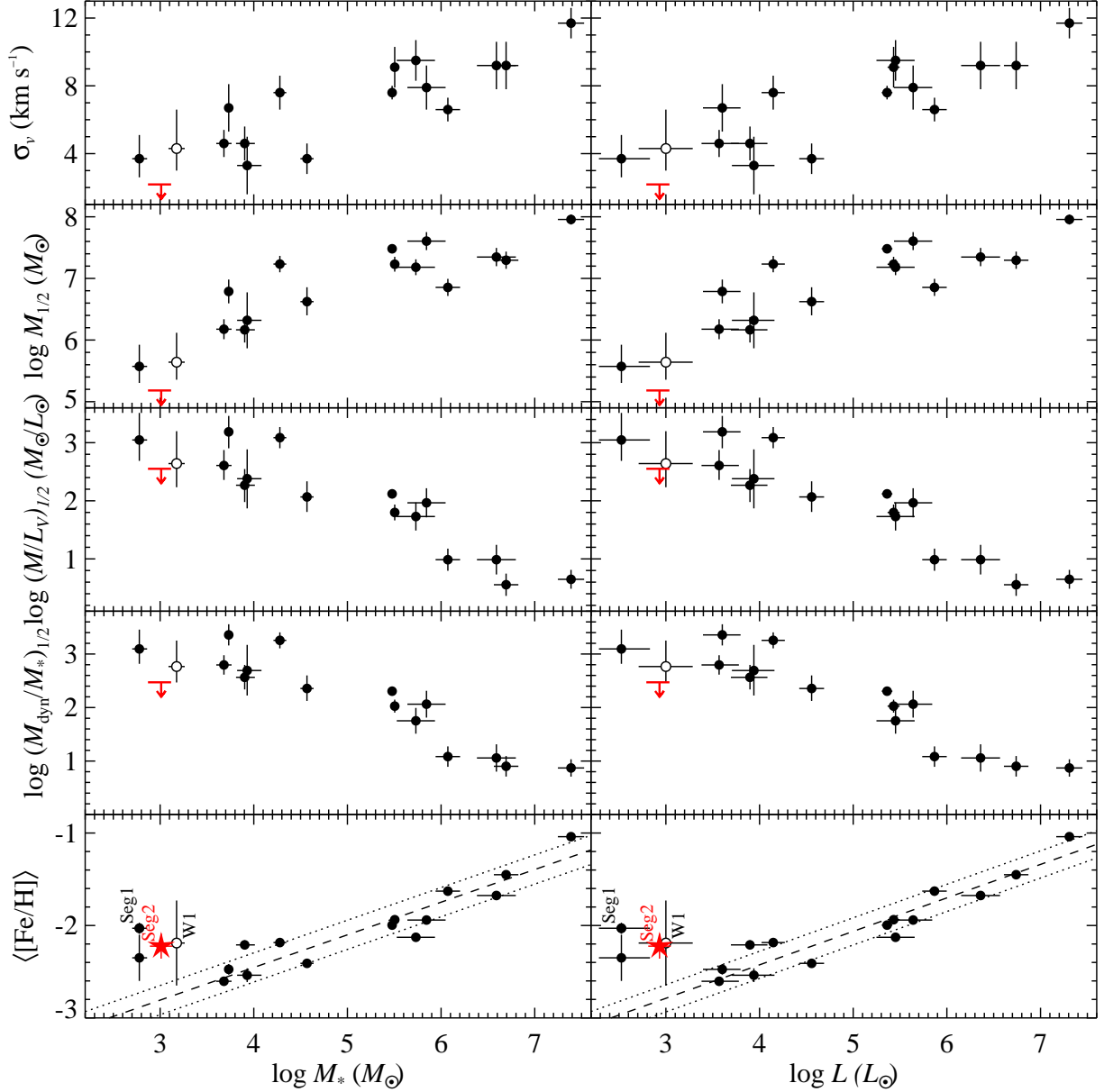


Figure 9. Velocity dispersion, mass within the half-light radius, mass-to-light ratio within the half-light radius, dynamical-to-stellar mass ratio within the half-light radius, and average metallicity versus stellar mass (left) and luminosity (right) for dwarf galaxies in the Local Group. Segue 2’s upper limits at 90% confidence are represented by red, downward-pointing arrows in the top four panels. Segue 2 is represented by a red star in the bottom panel. Willman 1 is represented by an open circle because it may not be in dynamical equilibrium (Willman et al. 2011). The dashed lines in the bottom panels are the linear regressions taking into account errors on both the x and y axes (Akritas & Bershady 1996). The dotted lines show the rms about the regression. Dynamical quantities (σ_v , $M_{1/2}$, $(M/L_V)_{1/2}$, and $(M_{\text{dyn}}/M_*)_{1/2}$) were taken from McConnachie (2012) and references therein. The stellar masses were taken from Woo et al. (2008) for the larger dSphs and Martin et al. (2008, using the values derived with the Kroupa et al. 1993 initial mass function) for the ultra-faint dSphs. The metallicity for Segue 1 is given twice for the two most recent measurements (Simon et al. 2011; Vargas et al. 2013). The other metallicities came from Willman et al. (2011, Willman 1) and Kirby et al. (2011b, other galaxies).

Segue 2 has a measurable spread in metallicity ($\sigma([\text{Fe}/\text{H}]) = 0.43$). The spread could be caused by gradual SN enrichment or inhomogeneous mixing. Inhomogeneous mixing is especially important for low-mass, low-metallicity galaxies (Greif et al. 2010; Ritter et al. 2012; Wise et al. 2012). Frebel & Bromm (2012) described the effect on chemical abundance patterns of “one-shot” chemical enrichment from a single generation of long-lived stars. The near instantaneousness of the enrichment would limit the dispersion in ratios of heavy ele-

ments, like $[\text{Si}/\text{Fe}]$, but the inhomogeneity could cause large spreads in metallicity indicators, like $[\text{Fe}/\text{H}]$. Figure 11 shows that Segue 2 has dispersion in both $[\text{Fe}/\text{H}]$ and heavy element ratios like $[\text{Si}/\text{Fe}]$. Therefore, we rule out inhomogeneous mixing as the source of the metallicity spread.

Instead, the dispersion in metallicity indicates that Segue 2 retained SN ejecta despite its small mass. This dispersion stands in contrast to an ultra-faint globular cluster, like Segue 3 ($\langle[\text{Fe}/\text{H}]\rangle = -1.7$, $\sigma([\text{Fe}/\text{H}]) \lesssim 0.3$,

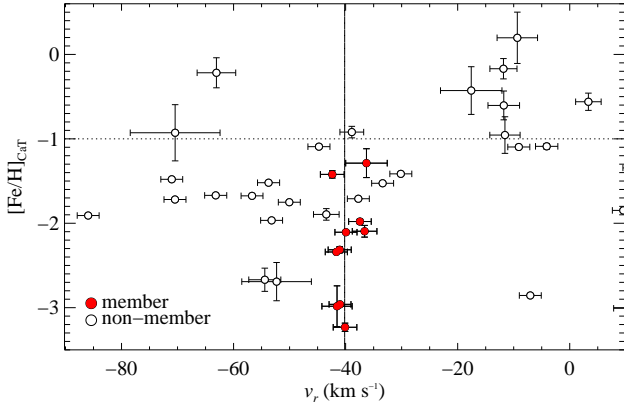


Figure 10. Ca triplet metallicity as a function of radial velocity for stars that pass all membership cuts except CMD, metallicity, and velocity. Member stars that pass all membership cuts are indicated by solid red points. The vertical dashed line represents $\langle v_{\text{helio}} \rangle$. The horizontal dotted line represents the metallicity cut for membership, but that cut is based on $[\text{Fe}/\text{H}]_{\text{syn}}$, not $[\text{Fe}/\text{H}]_{\text{CaT}}$.

Fadely et al. 2011). A galaxy with the 90% C.L. upper limit on Segue 2’s velocity dispersion (2.2 km s^{-1}) could not have survived the energy input of even a single SN. The SN would inject $E_{\text{SN}} = 8.5 \times 10^{49}$ erg of kinetic energy into the galaxy (Thornton et al. 1998). The SN would unbind $M_{\text{ej}} = E_{\text{ej}}/(6\sigma_v^2) = 1.5 \times 10^5 M_{\odot}$ of gas from the galaxy. That mass is 150 times larger than the present stellar mass. The galaxy must have had much more mass at the time of star formation than its present stellar mass. The source of this mass could be dark matter or stars that were part of the galaxy before any possible tidal stripping (Section 6.1).

The mean metallicity of Segue 2 is $\langle [\text{Fe}/\text{H}] \rangle = -2.22 \pm 0.13$, almost the same as the more luminous MW satellite Ursa Minor ($\langle [\text{Fe}/\text{H}] \rangle = -2.13 \pm 0.01$, Kirby et al. 2011b). The similarity in metallicity is notable because Segue 2 is 330 times less luminous than Ursa Minor. According to the universal LZr for MW dSphs (Kirby et al. 2011b), an intact galaxy with the luminosity of Segue 2 should have a mean metallicity of $\langle [\text{Fe}/\text{H}] \rangle = -2.83$. The intrinsic 1σ scatter in the relation at fixed luminosity is 0.16 dex. Therefore, neither intrinsic scatter nor the error on the mean metallicity brings Segue 2 into agreement with the LZr. The bottom panels of Figure 9 show the discrepancy, expressed in terms of luminosity and stellar mass.

The deviation from the LZr is statistically highly significant. We sampled 10 metallicities from a probability distribution based on the closed box model of chemical evolution: $P([\text{Fe}/\text{H}]) = (\ln 10/p) 10^{[\text{Fe}/\text{H}]} \exp(-10^{[\text{Fe}/\text{H}]/p})$ (Lynden-Bell 1975; Pagel 1997). The effective yield, p , is related to the average metallicity by $\langle [\text{Fe}/\text{H}] \rangle = \log p - 0.251$. We repeated this sampling for 10^6 trials. For each trial, we sampled the luminosity of Segue 2 from a Gaussian distribution with a mean of $L = 900 L_{\odot}$ and a width of $200 L_{\odot}$. We chose the mean metallicity of the distribution according to the LZr. The average metallicity of the 10 stars met or exceeded the observed average metallicity of $\langle [\text{Fe}/\text{H}] \rangle = -2.22$ in 10 trials. We also replicated the exercise assuming that the true mean metallicity is 0.16 dex higher than the

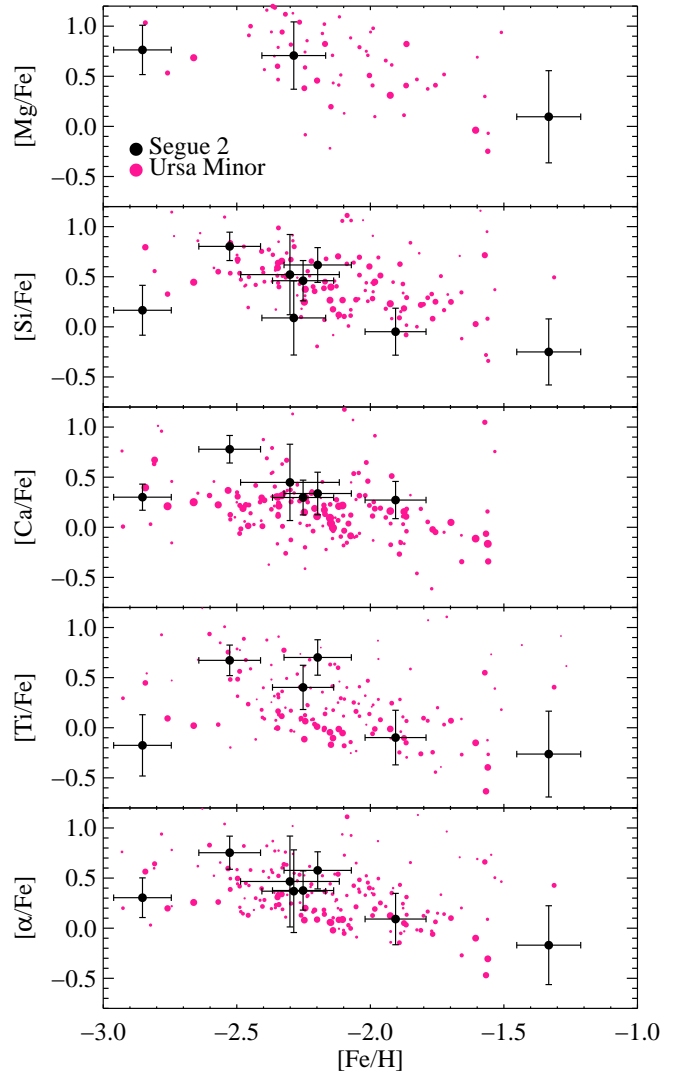


Figure 11. Distribution of individual $[\alpha/\text{Fe}]$ ratios in Segue 2 (black points) compared to Ursa Minor (magenta points, Kirby et al. 2011a), a dSph with an average metallicity similar to Segue 2. The bottom panel shows an average of the available $[\text{Mg}/\text{Fe}]$, $[\text{Si}/\text{Fe}]$, $[\text{Ca}/\text{Fe}]$, and $[\text{Ti}/\text{Fe}]$ ratios for each star. For Ursa Minor, larger points represent smaller measurement uncertainties.

LZr to account for the 1σ intrinsic scatter. In this case, 1786 trials out of 10^6 had $\langle [\text{Fe}/\text{H}] \rangle \geq -2.22$. Therefore, Segue 2 is a significant outlier from the LZr defined by more luminous dSphs. Its probability of conforming to the LZr is at most 0.2%.

The detailed abundance pattern of Segue 2 is also similar to Ursa Minor, measured by Kirby et al. (2011a). Figure 11 shows the comparison. The distributions are virtually indistinguishable. The similar offset and slope of the $[\alpha/\text{Fe}]$ vs. $[\text{Fe}/\text{H}]$ relation indicates a similar star formation history for Ursa Minor and Segue 2. Both galaxies seem to have had very low-level star formation with declining star formation rates (SFRs) for most of their lives. The weak star formation resulted in few Type II SNe, but the extent of star formation allowed the later generations of stars to incorporate the α -poor, Fe-rich ejecta from Type Ia SNe, which were delayed relative to Type II SNe. As a result, the $[\alpha/\text{Fe}]$ ratios de-

clined over time as $[\text{Fe}/\text{H}]$ increased. The slopes in Figure 11 for both Segue 2 and Ursa Minor are close to -1 , which indicates that the metallicity evolution was driven almost entirely by Fe and not the α elements. This can happen only when the SFR is so low that the frequency of Type Ia SNe completely dominates over Type II SNe after the first generation of stars. Furthermore, we can deduce that the onset of Type Ia SNe occurred at low metallicity in both galaxies ($[\text{Fe}/\text{H}] < -2.5$) because a plateau of $[\alpha/\text{Fe}]$ is not detectable at higher metallicities.

The decline of $[\alpha/\text{Fe}]$ with increasing metallicity shows that star formation in Segue 2 lasted for at least tens of Myr. The minimum delay time for a Type Ia SN is not well constrained, but it must be at least as long as the lifetime of a star with an initial mass of $8 M_{\odot}$, the maximum mass of a star that does not explode as a Type II SN. That lifetime is about 30 Myr (Matteucci & Greggio 1986). In reality, the galaxy needed to sustain several explosions of Type Ia SNe to achieve a steady decline in $[\alpha/\text{Fe}]$. As a result, the star formation lifetime is almost certainly at least several times 30 Myr.

Most other ultra-faint satellites share these properties. Vargas et al. (2013) showed that $[\alpha/\text{Fe}]$ ratios decline as a function of $[\text{Fe}/\text{H}]$ in six ultra-faint dwarfs. Segue 1 and Ursa Major II are possible exceptions. Type Ia SN enrichment seems to be a nearly universal phenomenon for dwarf galaxies, including ultra-faint dwarfs. In contrast, the chemical abundance patterns of almost all globular clusters do not show evidence for Type Ia SN enrichment.

The similarity of chemical properties, especially mean metallicity, to a more luminous satellite leads to two possible explanations for the origin of Segue 2. It could be that Segue 2 is a tidally stripped remnant (see Lokas et al. 2012) of a larger satellite. On the other hand, it is possible that galaxy formation has a lower bound in metallicity.

6.1. The Tidal Stripping Scenario

The similarity of the chemical properties of Ursa Minor and Segue 2 and the deviation from the LZR might indicate that Segue 2 is the remnant of a galaxy that has been tidally stripped by the MW. In this scenario, stars would have been removed from Segue 2 as it fell into the MW's gravitational potential. It would lose stellar mass and luminosity as it dissolved, but its stars' chemical properties would not have changed. Therefore, it would move to the left in the bottom panels of Figure 9. For example, suppose that Segue 2 was a dSph identical to Ursa Minor before it fell into the MW. Its initial luminosity would be $2.8 \times 10^5 L_{\odot}$ (Irwin & Hatzidimitriou 1995). If it lost 99.7% of its stellar mass, it would appear as B09 and we have observed Segue 2.

Tidal stripping of some dwarf galaxies certainly happens. It can be dramatic, as is the case for the Sagittarius dSph. Sagittarius has tidal tails that span the entire sky (Ibata et al. 2002; Majewski et al. 2003), and it likely deposited many of the MW halo's globular clusters in the process of dissolution (Law & Majewski 2010). Tidal stripping can also be subtle and result only in stellar overdensities with cold velocity dispersions (Schlaufman et al. 2009). If the MW is tidally stripping Segue 2, then it falls into the latter category of subtle disruption, although B09 suggested that Segue 2 was deposited into the MW halo by a larger host, just as Sagit-

tarius has deposited globular clusters.

Peñarrubia et al. (2008a) showed from N -body simulations that the M/L will increase as dwarf galaxies become tidally stripped. They assumed that the stars follow cored King (1962) profiles and that the dark matter follows a cusped NFW (Navarro et al. 1997) profile. In this case, the galaxy would need to lose nearly all of its mass in both dark matter and stars in order to end up like Segue 2. More than 90% of the dark matter needs to be stripped before the stars are affected. In order to lose 99.7% of its stellar mass, the galaxy would have to lose $> 99.9\%$ of its dark matter (Peñarrubia et al. 2008b). However, the dark matter subhalos of dwarf galaxies may not follow NFW cusps (i.e., de Blok 2010), in which case both the stars and dark matter would be more fragile. In the case of a cored dark matter profile, Segue 2 could not have been stripped to its present state without being completely disrupted. In the case of a cusped halo, Segue 2 could be the whittled center of a galaxy once the size of Ursa Minor. Segue 2 may also have its own yet-undetected, low-surface brightness, low-metallicity tidal tails.

The properties of Segue 2 are mostly consistent with the tidal stripping scenario except that its half-light radius is very small. Peñarrubia et al. (2008b) showed that intense tidal stripping of 99% to 99.9% of the stellar mass of a dSph decreases the surface brightness by a factor of ~ 300 , increases the mass-to-light ratio by a factor of ~ 10 , decreases the velocity dispersion by a factor of ~ 6 , and decreases the half-light radius by a factor of ~ 1.5 . All of these except the half-light radius are roughly consistent with transforming Ursa Minor into Segue 2 via tidal stripping. The observed half-light radius of Segue 2 (34 pc) is a factor of 3–4 too small. However, Peñarrubia et al. (2008b) considered only six models of dwarf satellite galaxies. A larger parameter space might include galaxies whose half-light radii are reduced enough to explain Segue 2 within the tidal stripping scenario.

In the tidal disruption scenario, the upper limits on the dynamical quantities that we calculated from the upper limit on the velocity dispersion may be incorrect. The upper limit on the mass estimate assumed that the galaxy is in dynamical equilibrium and is supported by velocity dispersion. If Segue 2 is instead an unbound tidal stream or loosely bound galaxy, then the mass estimate is unreliable. Nonetheless, the upper limits for the dynamical quantities for Segue 2 are consistent with the same relationships between dynamical quantities and luminosity or stellar mass as other dwarf galaxies (Figure 9).

6.2. A Metallicity Floor for Galaxy Formation

An alternative explanation for the chemical composition and low luminosity of Segue 2 is that the stellar content of the galaxy is bound and largely unaffected by tidal stripping. Instead, the galaxy formed only $1000 M_{\odot}$ of stars over its entire lifetime. In this case, the comparatively high metallicity of the galaxy needs to be explained.

Segue 2 is not alone in lying above the LZR. The ultra-faint satellites Segue 1 and Willman 1 also might be more metal-rich than their luminosities would suggest from an extrapolation of the LZR. Segue 1 con-

tains an extremely metal-poor star ($[\text{Fe}/\text{H}] = -3.3 \pm 0.2$, Geha et al. 2009). However, more recent spectroscopy (Simon et al. 2011) of more stars found a mean metallicity of $\langle [\text{Fe}/\text{H}] \rangle = -2.38 \pm 0.37$. Vargas et al. (2013) independently measured $\langle [\text{Fe}/\text{H}] \rangle = -2.03 \pm 0.06$ from the same spectra of Segue 1 stars. Norris et al. (2010) also derived $\langle [\text{Fe}/\text{H}] \rangle = -2.7 \pm 0.4$ from Ca H and K absorption rather than Fe I lines. For its luminosity (Martin et al. 2008), Segue 1 should have a mean metallicity of $\langle [\text{Fe}/\text{H}] \rangle = -2.98$. Simon et al.’s measurements are marginally consistent with the LZR, taking into account the error on the mean and the intrinsic scatter in the relation. On the other hand, Segue 1 is a highly significant outlier based on Vargas et al.’s measurements. Willman 1 is another satellite that might lie above the LZR. Unfortunately, there are only two known red giants in the galaxy, and their average metallicity is $\langle [\text{Fe}/\text{H}] \rangle = -2.19 \pm 0.46$ (Willman et al. 2011). Based on its luminosity, it should have $\langle [\text{Fe}/\text{H}] \rangle = -2.81$. Furthermore, the galaxian nature of Willman 1 is uncertain. The velocity distribution of its stars is irregular and non-Gaussian (Willman et al. 2011). It may not be in dynamical equilibrium, and it could be a tidally stripped remnant, such as we proposed for Segue 2 in Section 6.1.

It is not practical to draw strong conclusions from only three galaxies that disobey the LZR. However, Segue 1, Segue 2, and Willman 1 together invoke the suggestion of a metallicity floor for galaxy formation. Simon & Geha (2007) first noticed that the ultra-faint galaxies lie slightly above the LZR. However, they used a metallicity indicator that has since been shown to be unreliable for very metal-poor stars. Kirby et al. (2011a) recomputed average metallicities based on Fe I lines, and they noticed a subtle change in the slope of the LZR around $10^5 L_{\odot}$ in the sense that the ultra-faint galaxies lay slightly above the LZR extrapolated from higher luminosities.

There is a theoretical reason to expect a metallicity floor for galaxy formation. A single pair instability SN can bring the metallicity of the interstellar medium of a galaxy to about one thousandth of the solar value ($10^{-3} Z_{\odot}$) and mark the transition from Population III to II star formation (Wise et al. 2012). Although one thousandth of the solar metallicity is not far from the metallicity floor that we observed ($[\text{Fe}/\text{H}] \approx -2.5$), some dwarf galaxies have stars with metallicities a factor of ten below that floor (e.g., Frebel et al. 2010; Tafelmeyer et al. 2010). As Wise et al. pointed out, the transition from Population III to II may not be reflected in a hard boundary in metallicity. But it could be reflected in a floor for the average metallicities of galaxies. Damped Lyman α systems (DLAs) at redshifts of $2.5 < z < 5$, which are presumably nascent galaxies, do not exhibit metallicities below 10^{-3} of the solar metallicity (Prochaska et al. 2003; Rafelski et al. 2012). It is conceivable that galaxies do not form unless they achieve this threshold metallicity. However, DLAs have much larger gas masses than the stellar mass of Segue 2.

We reiterate that it is unwise to make much of the sparse sampling of the LZR at $L < 10^4 L_{\odot}$. It would be wise to expand the sample sizes in Segue 1, Segue 2, and Willman 1 before we conclude that the linearity of the LZR disappears below a few thousand L_{\odot} . Nonetheless, it is interesting to consider the bottom panels of Figure 9

together with the metallicity floor for DLAs.

7. RELEVANCE TO DARK MATTER PHYSICS

The two models presented in the previous section for the origin of Segue 2’s high metallicity given its luminosity have very different implications for our understanding of galaxy formation and cold dark matter (CDM) models. In this section, we address Segue 2’s place in the Λ CDM paradigm.

In Section 6.1, we suggested that Segue 2 may be the remnant of a galaxy that was previously 100–1000 times more luminous than it is now. Furthermore, we inferred from its retention of supernova ejecta that it was once hosted by a substantial dark matter halo. If so, then Segue 2 is the first known galaxy to have shed its dark matter halo without being completely disrupted. To be consistent with a progenitor similar to Ursa Minor, which provides a good match for the average metallicity and abundance ratios, Segue 2 would have once been hosted by a halo with a maximum circular velocity of $v_{\text{max}} \approx 20 - 25 \text{ km s}^{-1}$, corresponding to a virial mass of $M_{\text{vir}} \approx (1 - 3) \times 10^9 M_{\odot}$ (Boylan-Kolchin et al. 2012).

By number, such objects should be rare—but not extremely rare—in the MW at $z = 0$. The Aquarius simulations (Springel et al. 2008) have between 60 and 110 distinct objects within 300 kpc of the halo center at $z = 0$ that were once at least this massive (Boylan-Kolchin et al. 2012, Table 1). However, most of these reside at large distances from their halo’s center and have apocenter-to-pericenter ratios around 6 : 1, which is not conducive to strong tidal stripping. The ratio needed to achieve stripping of 99.7% of the stars (to transform an Ursa Minor-like dSph into Segue 2) would have to be about 50 : 1 (Peñarrubia et al. 2008b). Only a small fraction of subhalos have orbital eccentricities that large. Those subhalos would spend most of their lives at large Galactocentric distances. As a result, galaxies similar to Segue 2 would be difficult to detect, and Segue 2 would likely be one of the closest such objects to the MW’s center. Furthermore, extremely tidally stripped galaxies likely would not survive their next 1–2 pericentric passages, which would make Segue 2 a transient phenomenon that will survive for only 2–3 Gyr. Proper motion studies of Segue 2 would be valuable in establishing whether its orbit is consistent with the tidal stripping hypothesis.

Even in the absence of proper motions, the Galactic coordinates ($l = 149^{\circ}$, $b = -38^{\circ}$) and Galactocentric distance (41 kpc) of Segue 2 exclude it from being a member of the MW’s “disk of satellites” suggested by Metz et al. (2007). The disk is ~ 20 kpc thick, and its pole points toward $l = 158^{\circ}$, $b = -12^{\circ}$. Metz et al. claimed that the existence of the plane was inconsistent with CDM structure formation. Segue 2’s location does not invalidate the plane of satellites because many of the MW’s satellites, including the most luminous satellites, do lie in the plane. However, Segue 2 could not be a tidal dwarf galaxy that came from the merger event that Metz et al. proposed to explain the orientation of the plane-aligned satellites.

In Section 6.2, we presented an alternate scenario, wherein Segue 2 is not a heavily-stripped remnant of a more massive galaxy but instead a relatively undisturbed dwarf galaxy whose properties indicate the existence of

a metallicity floor in galaxy formation. The implications for Λ CDM galaxy formation in this scenario are very different from the tidal stripping scenario. Segue 2 would have been born in a very low-mass dark matter halo of $v_{\max} \lesssim 8 \text{ km s}^{-1}$. The MW is predicted to host at least 1000 such dark matter subhalos at present in CDM models (Diemand et al. 2008; Springel et al. 2008). Either Segue 2 would be the first of a vast class of new galaxies to be discovered with very low luminosities and very low dark matter content, or it would have to represent a rare case of a dark matter halo that is typically too small to host a galaxy but, for some reason, managed to form a small number of stars over at least 100 Myr.

The presence of stars in a subhalo as small as $v_{\max} = 8 \text{ km s}^{-1}$ is especially remarkable because the threshold for atomic cooling to form stars is $v_{\max} > 17 \text{ km s}^{-1}$ (Rees & Ostriker 1977). Expressed in terms of virial temperature, Segue 2 has $T_{\text{vir}} < 2400 \text{ K}$, whereas the atomic hydrogen cooling threshold is 10^4 K . As a result, the gas in Segue 2 would have had to undergo molecular (H_2) cooling in order to form stars. If the mass of the subhalo when it formed stars was as low as it is today, then Segue 2 would be the only known galaxy that must have experienced only molecular cooling without atomic cooling.

If Segue 2’s dark matter halo has not been heavily affected by Galactic tides, then its existence might provide an interesting constraint on Warm Dark Matter (WDM) models because it has a low halo mass ($v_{\max} < 8 \text{ km s}^{-1}$). The formation of halos with $v_{\max} \sim 8 \text{ km s}^{-1}$ should be strongly suppressed for thermal WDM particles with $m_{\text{WDM}} \sim 4 \text{ keV}$ (Schneider et al. 2013; Angulo et al. 2013), comparable to published lower limits based on the Lyman α forest (Viel et al. 2009). The existence of galaxies in very low mass dark matter halos would favor models with significant small-scale power (e.g., CDM), and counts of such objects may provide the strongest lower limits on the thermal mass of dark matter particles (Polisensky & Ricotti 2011). However, more work is needed to clarify the extent to which halo formation is suppressed below the associated filtering scale in the power spectrum (Angulo et al. 2013).

8. SUMMARY

Belokurov et al. (2009) discovered the Segue 2 ultra-faint dwarf galaxy in SEGUE photometry. From the line-of-sight stellar velocity dispersion measured with MMT/Hectospec, they determined that its mass has a much larger fraction of dark matter than of stars. They also found evidence for a tidal stream at the same position and radial velocity as Segue 2.

We observed Segue 2 with ten Keck/DEIMOS slit-masks in order to enlarge the sample of radial velocities, refine the mass estimate, and add metallicity and detailed chemical abundances to the available data. We measured radial velocities by cross-correlation with template spectra, and we estimated velocity uncertainties by Monte Carlo resampling of the spectra based on a noise model of the full spectrum. We measured Mg, Si, Ca, Ti, and Fe abundances by comparing the observed spectra to synthetic spectra using χ^2 minimization.

With our threefold increase in spectroscopic sample size, we could not confirm B09’s measurements of ve-

locity dispersion ($3.4_{-1.2}^{+2.5} \text{ km s}^{-1}$) and mass ($5.5_{-3.1}^{+10.5} \times 10^5 M_{\odot}$). Instead, we placed an upper limit on the stellar line-of-sight velocity dispersion of $\sigma_v < 2.2$ (2.6) km s^{-1} with 90% (95%) confidence. The inferred limit on the mass within the half-light radius is $M_{1/2} < 1.5$ (2.1) $\times 10^5 M_{\odot}$.

We found a dispersion in $[\text{Fe}/\text{H}]$ and a decline of $[\alpha/\text{Fe}]$ as a function of $[\text{Fe}/\text{H}]$. These two chemical properties establish that Segue 2 retained SN ejecta and that star formation lasted for at least several generations of Type Ia SNe (at least 100 Myr). We also determined that the average metallicity of Segue 2 places it more metal-rich than the LZR defined by the more luminous MW satellite galaxies. The $[\alpha/\text{Fe}]$ ratios as a function of metallicity are indistinguishable from the more luminous dSph Ursa Minor.

Taken together, the dynamical and chemical characteristics of Segue 2 point to two possible scenarios for its formation. Segue 2 could be the barest remnant of a galaxy that once had a luminosity of $2 \times 10^5 L_{\odot}$. Gravitational interaction with the MW’s gravitational potential removed nearly all of its stars and dark matter halo, leaving only the dense center of the galaxy. On the other hand, Segue 2 could have formed with its present stellar mass and metallicity. This scenario has been proposed for the ultra-faint galaxy Segue 1 (Geha et al. 2009; Simon et al. 2011). The deviation from the LZR might indicate a metallicity floor for galaxy formation, which is evocative of the metallicity floor observed for damped Lyman α systems at high redshift (Prochaska et al. 2003; Rafelski et al. 2012).

Overall, the tidal stripping scenario seems more plausible. The metallicity floor scenario must overcome the fact that dSphs contain extremely metal-poor stars and that there are ultra-faint galaxies, like Coma Berenices ($\langle [\text{Fe}/\text{H}] \rangle = -2.60 \pm 0.05$, Kirby et al. 2011a), with metallicities below that of Segue 2. On the other hand, SDSS has revealed copious evidence of ongoing tidal stripping of satellites, and Segue 2 may not have been immune to the same fate. The distinguishing characteristic of Segue 2 is that the MW’s tides have likely whittled it down to the least massive galaxy known. The tidal stripping scenario still needs to overcome the discrepancy between the half-light radius of models of tidally stripped dSphs (Peñarrubia et al. 2008b) and the observed half-light radius of Segue 2. It would be interesting to explore a larger parameter space of initial galaxy shapes (such as the recent simulations of Kazantzidis et al. 2013) to test whether tidal stripping of a dSph with the stellar mass of Ursa Minor could produce Segue 2.

On a final note, we reached the limit of measuring a galaxy’s velocity dispersion with DEIMOS. Resolving the dispersion of Segue 2 will require higher resolution spectroscopy. High-resolution spectrographs like Keck/HIRES and Subaru/HDS could possibly measure the velocity distribution of ~ 10 stars in Segue 2 over 3–4 nights. However, new surveys like LSST and SkyMapper will discover new tiny galaxies, some of which may have velocity dispersions too small to be resolved with medium-resolution, multi-object spectrographs. These tiny galaxies and their relevance to dark matter physics make a compelling case for building high-resolution spectrographs for the next generation of extremely large tele-

scopes. The combination of collecting area and spectral resolution will allow measurements of the velocities of the fainter, more common stars in Segue 2 and undiscovered galaxies like it. Only then can we measure their dynamical masses.

We are grateful to the many people who have worked to make the Keck Telescope and its instruments a reality and to operate and maintain the Keck Observatory. The authors wish to extend special thanks to those of Hawaiian ancestry on whose sacred mountain we are privileged to be guests. Without their generous hospitality, none of the observations presented herein would have been possible.

We thank the anonymous referee for a courteous report on our article and Josh Simon for a helpful discussion. We are also grateful to Shunsaku Horiuchi for confirming that Segue 2 shows no signal in sky maps from the *Fermi* Gamma Ray Space Telescope. ENK and MBK acknowledge support from the Southern California Center for Galaxy Evolution, a multicampus research program funded by the University of California Office of Research, and partial support from NSF grant AST-1009973. JGC thanks NSF grant AST-0908139 for partial support.

Facility: Keck:II (DEIMOS)

REFERENCES

- Abazajian, K. N., Adelman-McCarthy, J. K., Agüeros, M. A., et al. 2009, *ApJS*, 182, 543
- Akritas, M. G., & Bershadsky, M. A. 1996, *ApJ*, 470, 706
- Angulo, R. E., Hahn, O., & Abel, T. 2013, *MNRAS*, submitted, arXiv:1304.2406
- Belokurov, V., Walker, M. G., Evans, N. W., et al. 2009, *MNRAS*, 397, 1748 (B09)
- Belokurov, V., Zucker, D. B., Evans, N. W., et al. 2007, *ApJ*, 654, 897
- Boettcher, E., Willman, B., Fadely, R., et al. 2013, *AJ*, submitted
- Boylan-Kolchin, M., Bullock, J. S., & Kaplinghat, M. 2012, *MNRAS*, 422, 1203
- Cooper, M. C., Newman, J. A., Davis, M., Finkbeiner, D. P., & Gerke, B. F. 2012, *Astrophysics Source Code Library*, 3003
- Davis, M., Faber, S. M., Newman, J., et al. 2003, *Proc. SPIE*, 4834, 161
- de Blok, W. J. G. 2010, *Advances in Astronomy*, 2010, 789293
- Deason, A. J., Belokurov, V., Evans, N. W., Watkins, L. L., & Fellhauer, M. 2012, *MNRAS*, 425, L101
- Demarque, P., Woo, J.-H., Kim, Y.-C., & Yi, S. K. 2004, *ApJS*, 155, 667
- Diemand, J., Kuhlen, M., Madau, P., et al. 2008, *Nature*, 454, 735
- Faber, S. M., Phillips, A. C., Kibrick, R. I., et al. 2003, *Proc. SPIE*, 4841, 1657
- Fadely, R., Willman, B., Geha, M., et al. 2011, *AJ*, 142, 88
- For, B.-Q., Sneden, C., & Preston, G. W. 2011, *ApJS*, 197, 29
- Frebel, A., & Bromm, V. 2012, *ApJ*, 759, 115
- Frebel, A., Kirby, E. N., & Simon, J. D. 2010, *Nature*, 464, 72
- Geha, M., Willman, B., Simon, J. D., et al. 2009, *ApJ*, 692, 1464
- Girardi, L., Bertelli, G., Bressan, A., et al. 2002, *A&A*, 391, 195
- Greif, T. H., Glover, S. C. O., Bromm, V., & Klessen, R. S. 2010, *ApJ*, 716, 510
- Ibata, R. A., Lewis, G. F., Irwin, M. J., & Cambrésy, L. 2002, *MNRAS*, 332, 921
- Illingworth, G. 1976, *ApJ*, 204, 73
- Irwin, M., & Hatzidimitriou, D. 1995, *MNRAS*, 277, 1354
- Jordi, K., Grebel, E. K., & Ammon, K. 2006, *A&A*, 460, 339
- Kazantzidis, S., Lokas, E. L., & Mayer, L. 2013, *ApJ*, 764, L29
- King, I. 1962, *AJ*, 67, 471
- Kirby, E. N., Cohen, J. G., & Bellazzini, M. 2012, *ApJ*, 751, 46
- Kirby, E. N., Cohen, J. G., Smith, G. H., et al. 2011a, *ApJ*, 727, 79
- Kirby, E. N., Guhathakurta, P., Simon, J. D., et al. 2010, *ApJS*, 191, 352
- Kirby, E. N., Guhathakurta, P., & Sneden, C. 2008, *ApJ*, 682, 1217
- Kirby, E. N., Lanfranchi, G. A., Simon, J. D., Cohen, J. G., & Guhathakurta, P. 2011b, *ApJ*, 727, 78
- Kroupa, P., Tout, C. A., & Gilmore, G. 1993, *MNRAS*, 262, 545
- Majewski, S. R., Skrutskie, M. F., Weinberg, M. D., & Ostheimer, J. C. 2003, *ApJ*, 599, 1082
- Law, D. R., & Majewski, S. R. 2010, *ApJ*, 718, 1128
- Lokas, E. L., Kazantzidis, S., & Mayer, L. 2012, *ApJ*, 751, L15
- Lynden-Bell, D. 1975, *Vistas in Astronomy*, 19, 299
- Martin, N. F., de Jong, J. T. A., & Rix, H.-W. 2008, *ApJ*, 684, 1075
- Martinez, G. D., Minor, Q. E., Bullock, J., et al. 2011, *ApJ*, 738, 55
- Matteucci, F., & Greggio, L. 1986, *A&A*, 154, 279
- McConnachie, A. W. 2012, *AJ*, 144, 4
- McConnachie, A. W., & Côté, P. 2010, *ApJ*, 722, L209
- Metz, M., Kroupa, P., & Jerjen, H. 2007, *MNRAS*, 374, 1125
- Navarro, J. F., Frenk, C. S., & White, S. D. M. 1997, *ApJ*, 490, 493
- Newman, J. A., Cooper, M. C., Davis, M., et al. 2013, *ApJS*, submitted, arXiv:1203.3192
- Norris, J. E., Wyse, R. F. G., Gilmore, G., et al. 2010, *ApJ*, 723, 1632
- Pagel, B. E. J. 1997, *Nucleosynthesis and Chemical Evolution of Galaxies* (Cambridge UP)
- Peñarrubia, J., McConnachie, A. W., & Navarro, J. F. 2008a, *ApJ*, 672, 904
- Peñarrubia, J., Navarro, J. F., & McConnachie, A. W. 2008b, *ApJ*, 673, 226
- Polisensky, E., & Ricotti, M. 2011, *Phys. Rev. D*, 83, 043506
- Preston, G. W. 1964, *ARA&A*, 2, 23
- Preston, G. W., & Paczynski, B. 1964, *ApJ*, 140, 181
- Prochaska, J. X., Gawiser, E., Wolfe, A. M., Cooke, J., & Gelino, D. 2003, *ApJS*, 147, 227
- Rafelski, M., Wolfe, A. M., Prochaska, J. X., Neeleman, M., & Mendez, A. J. 2012, *ApJ*, 755, 89
- Rees, M. J., & Ostriker, J. P. 1977, *MNRAS*, 179, 541
- Regnault, N., Conley, A., Guy, J., et al. 2009, *A&A*, 506, 999
- Ritter, J. S., Safrank-Shrader, C., Gnat, O., Milosavljević, M., & Bromm, V. 2012, *ApJ*, 761, 56
- Robin, A. C., Reylé, C., Derrière, S., & Picaud, S. 2003, *A&A*, 409, 523
- Rockosi, C. M., Odenkirchen, M., Grebel, E. K., et al. 2002, *AJ*, 124, 349
- Schlaufman, K. C., Rockosi, C. M., Allende Prieto, C., et al. 2009, *ApJ*, 703, 2177
- Schneider, A., Smith, R. E., & Reed, D. 2013, *MNRAS*, submitted, arXiv:1303.0839
- Sesar, B. 2012, *AJ*, 144, 114
- Simon, J. D., & Geha, M. 2007, *ApJ*, 670, 313
- Simon, J. D., Geha, M., Minor, Q. E., et al. 2011, *ApJ*, 733, 46
- Sohn, S. T., Majewski, S. R., Muñoz, R. R., et al. 2007, *ApJ*, 663, 960
- Springel, V., Wang, J., Vogelsberger, M., et al. 2008, *MNRAS*, 391, 1685
- Starkenburg, E., Hill, V., Tolstoy, E., et al. 2010, *A&A*, 513, A34
- Tafelmeyer, M., Jablonka, P., Hill, V., et al. 2010, *A&A*, 524, A58
- Thornton, K., Gaudlitz, M., Janka, H.-T., & Steinmetz, M. 1998, *ApJ*, 500, 95
- Vargas, L. C., Geha, M., Kirby, E. N., & Simon, J. D. 2013, *ApJ*, 767, 134
- Viel, M., Bolton, J. S., & Haehnelt, M. G. 2009, *MNRAS*, 399, L39
- Walker, M. G., Belokurov, V., Evans, N. W., et al. 2009, *ApJ*, 694, L144
- Walker, M. G., Mateo, M., Olszewski, E. W., et al. 2006, *AJ*, 131, 2114
- Walsh, S. M., Willman, B., & Jerjen, H. 2009, *AJ*, 137, 450
- Willman, B., Geha, M., Strader, J., et al. 2011, *AJ*, 142, 128
- Willman, B., & Strader, J. 2012, *AJ*, 144, 76
- Wise, J. H., Turk, M. J., Norman, M. L., & Abel, T. 2012, *ApJ*, 745, 50
- Wolf, J., Martinez, G. D., Bullock, J. S., et al. 2010, *MNRAS*, 406, 1220
- Woo, J., Bourteau, S., & Dekel, A. 2008, *MNRAS*, 390, 1453
- Yanny, B., Rockosi, C., Newberg, H. J., et al. 2009, *AJ*, 137, 4377
- Zucker, D. B., Belokurov, V., Evans, N. W., et al. 2006, *ApJ*, 643, L103

Table 2
 Target List

ID	g_0 (mag)	i_0 (mag)	Masks ^a	S/N (\AA^{-1})	v_r (km s^{-1})	EW(Na I 8190) (\AA)	[Fe/H] (dex)	Member?	Reason ^b
SDSS J021908.97+201948.9	23.091 ± 0.331	19.745 ± 0.036	1	52.2	-65.5 ± 2.0	N	CMD v_r
SDSS J021909.11+201115.9	21.178 ± 0.075	20.836 ± 0.101	1	17.4	-43.2 ± 10.7	Y	
SDSS J021909.23+200552.8	25.405 ± 0.426	21.478 ± 0.184	1	17.1	$+32.0 \pm 3.0$	N	CMD v_r
SDSS J021909.29+201958.7	22.572 ± 0.219	23.509 ± 0.721	1	0.3	N	CMD Bad
SDSS J021909.34+200045.5	24.447 ± 0.568	21.909 ± 0.201	1	6.2	N	CMD Bad
SDSS J021909.53+200056.5	21.681 ± 0.107	19.389 ± 0.025	1	63.4	$+35.1 \pm 2.0$	N	CMD v_r
SDSS J021909.84+201122.7	22.818 ± 0.294	20.507 ± 0.073	1	8.2	$+28.6 \pm 5.0$	N	CMD v_r
SDSS J021909.97+201254.0	20.252 ± 0.033	19.575 ± 0.032	2	49.4	-42.4 ± 2.1	...	-1.33 ± 0.12	Y	
SDSS J021910.17+201539.1	24.182 ± 5.490	17.341 ± 0.013	1	110.5	$+13.6 \pm 2.0$	N	CMD v_r
SDSS J021910.22+200324.8	19.593 ± 0.021	19.374 ± 0.024	1	61.2	$+93.5 \pm 7.6$	N	CMD v_r
...

References. — Identifications and photometry from SDSS (Abazajian et al. 2009).

Note. — (This table is available in its entirety in a machine-readable form in the online journal. A portion is shown here for guidance regarding its form and content.)

^a Number of DEIMOS masks on which the object was observed.

^b Reasons for non-membership. CMD: Location in the color-magnitude diagram. v_r : Inappropriate radial velocity. Na: Spectrum shows strong Na I λ 8190 doublet. [Fe/H]: The measured metallicity is greater than [Fe/H] = -1.0 . G: Spectrum shows emission lines or redshifted Ca H and K lines, indicating that the object is a galaxy. Bad: Spectral quality was insufficient for radial velocity measurement.